Photoproduction of ϕ mesons from the proton: Polarization observables and strangeness in the nucleon

Alexander I. Titov,[1,*] Yongseok Oh,[2,†] Shin Nan Yang,[3,‡] and Tosiyuki Morii[4,§]
[1]*Bogoliubov Laboratory of Theoretical Physics, JINR, 141980 Dubna, Russia*
[2]*Research Institute for Basic Sciences and Department of Physics, Seoul National University, Seoul 151-742, Korea*
[3]*Department of Physics, National Taiwan University, Taipei, Taiwan 10617, Republic of China*
[4]*Faculty of Human Development, Kobe University, 3-11 Tsurukabuto, Nada, Kobe 675, Japan*
(Received 15 April 1998)

The polarization observables in ϕ meson photoproduction are studied to probe the strangeness content of the nucleon. In addition to the dominant diffractive production and the one-pion-exchange process, we take into account the direct knockout mechanism that arises from the possible hidden strangeness content of the nucleon. We find that some double polarization observables are very sensitive to the strangeness content of the proton because of the different spin structures of the amplitudes associated with different mechanisms. This suggests that such measurements could be very useful in probing the strangeness content in the proton. The orbitally excited quark-cluster configurations in the proton are included in the calculation and found to have little effect. [S0556-2813(98)06610-2]

PACS number(s): 13.88.+e, 24.70.+s, 25.20.Lj, 13.60.Le

I. INTRODUCTION

The possible existence of hidden strangeness in the nucleon has recently become one of the most controversial problems in nuclear/hadron physics. Some analyses of the pion-nucleon sigma term [1,2], polarized deep-inelastic lepton-proton scattering [3–5], and low energy elastic neutrino-proton scattering [6,7] indicate a significant role of strange sea quarks in the nucleon structure [8]. However, it has also been argued that such experimental results could be understood with little or null strangeness in the nucleon [9,10].

It will be interesting, therefore, to study other processes that might be related directly to the strangeness content of the nucleon [11–16]. One of them is ϕ meson production from the proton. Since the ϕ meson is a nearly pure $s\bar{s}$ state because of ideal mixing with the ω meson, its coupling to the proton is suppressed through the OZI rule. Then the idea is that we could extract information about the hidden strangeness of the nucleon by studying the strange sea quark contribution through the OZI evasion processes. One example is ϕ production in proton–anti-proton annihilation. Recent experiments on vector meson production through $\bar{p}p$ annihilation at rest [17–19] report a strong violation of the OZI rule. It can be accounted for by the presence of an intrinsic $s\bar{s}$ component in the nucleon wave function [8,20], which contributes to the process through the rearrangement and shake-out diagrams [21–24]. On the other hand, it was also claimed that this OZI violation could be explained through modified meson exchange models [25,26] without any strangeness content of the nucleon.

Another possibility is ϕ photo- and electro-production from proton targets [13]. In this process, in addition to the vector-meson dominance model (VDM), the contribution from the hidden strangeness of the proton arises through the direct knockout process. In Refs. [27,28], Henley *et al.* calculated the contribution from knockout process to ϕ electroproduction cross section and found it comparable to that of VDM with an assumption of a 10–20 % strange sea quark admixture in the proton wave function. To arrive at this conclusion, they used nonrelativistic quark model wave functions for the hadrons. However, since the kinematical region of ϕ meson production is beyond the applicability of the nonrelativistic quark model, the relativistic corrections are expected to be important. In Refs. [29,30] we improved the calculations of Refs. [27,28] with the use of a relativistic harmonic oscillator quark model (RHOQM). We found that the cross section of the direct knockout mechanism for the electroproduction is comparable to that of VDM at moderately large electron four-momentum transfer with less than 5% admixture of strange sea quarks in the proton. However, it is not easy to disentangle the two mechanisms from the cross section measurement because their respective contributions have similar dependence on momentum transfer [30].

To distinguish between the knockout and VDM processes, it was suggested the difference in the spin structures of various amplitudes be exploited [27,31–34]. In Ref. [33], we showed that some double polarization observables are indeed very sensitive to the hidden strangeness content of the proton. We found that, with the use of RHOQM, the direct knockout process gives a very distinct contribution to some of the double polarization observables in ϕ photoproducton as compared to those of diffractive production and one-pion-exchange (OPE) process. A similar conclusion was drawn from the $\bar{p}p \to \bar{\Lambda}\Lambda$ process to distinguish between contributions from the hidden strangeness of the nucleon and the effects from meson exchange processes [35]. (See also Ref. [36].) The one-pion-exchange process arises from the

*Electronic address: atitov@thsun1.jinr.ru
†Electronic address: yoh@phya.snu.ac.kr
‡Electronic address: snyang@phys.ntu.edu.tw
§Electronic address: morii@kobe-u.ac.jp

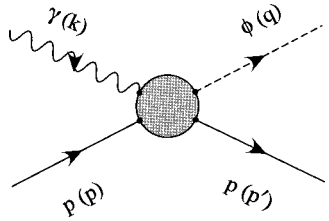

FIG. 1. Kinematics for ϕ meson photoproduction from the proton, $\gamma p \to \phi p$.

ϕ-π-$\rho(\gamma)$ coupling. Similar ω-π-$\rho(\gamma)$ coupling gives non-negligible effects in the ω-meson production case [37].

In this paper, we extend our previous work to discuss other spin observables in ϕ photoproduction and give the details which were left out in Ref. [33]. We also improve the VDM amplitude to take into account the gauge invariance requirement within a quark-Pomeron interaction picture. We further include, besides the lowest one, other configurations in the five-quark cluster model of the nucleon, which may give non-negligible contribution to the nucleon spin [20].

In Sec. II, we define the kinematical variables and briefly review the definitions of general spin observables in terms of helicity amplitudes. Section III is devoted to our model for ϕ photoproduction. We include the diffractive and OPE production processes as well as the direct knockout processes that arise from the hidden strangeness of the nucleon. The gauge invariance of VDM amplitude is discussed as well. Our results for the spin observables are presented in Sec. IV along with their dependence on the hidden strangeness content of the proton. In Sec. V we discuss the role of orbitally excited quark-cluster configurations in the nucleon wave function in ϕ photoproduction. We find that their effect is not important. Section VI contains summary and conclusion. Some detailed discussions and expressions for the physical parameters are given in Appendixes.

II. SPIN OBSERVABLES AND THE HELICITY AMPLITUDES

We first define the kinematical variables for ϕ photoproduction from the proton, $\gamma + p \to \phi + p$, as shown in Fig. 1. The four-momenta of the incoming photon, outgoing ϕ, initial (target) proton, and final (recoil) proton are k, q, p, and p', respectively. In the laboratory frame, we write $k=(E_\gamma^L,\mathbf{k}_L)$, $q=(E_\phi^L,\mathbf{q}_L)$, $p=(E_p^L,\mathbf{p}_L)$, and $p'=(E_{p'}^L,\mathbf{p}'_L)$. The variables in the c.m. system are written as $k=(\nu,\mathbf{k})$, $q=(E_\phi,\mathbf{q})$, $p=(E_p,-\mathbf{k})$, and $p'=(E_{p'},-\mathbf{q})$, respectively, as in Fig. 2. We also define $t=(p-p')^2$ and $W^2=(p+k)^2$ with M_N the nucleon mass, M_π the pion mass, and M_ϕ the ϕ mass. The differential cross section is given by

$$\frac{d\sigma}{d\Omega}=\rho_0\overline{|T_{fi}|^2}, \tag{2.1}$$

where $\rho_0=(M_N^2|\mathbf{q}|)/(16\pi^2W^2|\mathbf{k}|)$.

The general formalism for the spin observables of $\gamma+p\to\phi+p$ has been discussed extensively in the literature. For completeness, we briefly review here the density matrix formalism and refer the interested readers to Refs. [38–42] for details.

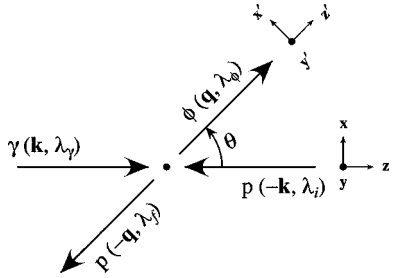

FIG. 2. The coordinate system and kinematical variables for ϕ meson photoproduction in the c.m. frame. θ is the scattering angle.

To study the spin observables, it is useful to work with the helicity amplitudes in the c.m. frame. For polarized ϕ meson photoproduction, $\vec{\gamma}+\vec{p}\to\vec{\phi}+\vec{p}$, the helicity amplitude takes the form

$$H_{\lambda_\phi,\lambda_f;\lambda_\gamma,\lambda_i}\equiv\langle\mathbf{q};\lambda_\phi,\lambda_f|T|\mathbf{k};\lambda_\gamma,\lambda_i\rangle, \tag{2.2}$$

where the variables and the coordinate systems are shown in Fig. 2 with λ_γ $(=\pm1)$, λ_ϕ $(=0,\pm1)$, and $\lambda_{i,f}$ $(=\pm1/2)$ denoting the helicities of the photon, ϕ meson, target proton, and recoil proton, respectively. We follow the Jacob-Wick phase convention [39,43] throughout this paper. In principle, there are $2\times2\times3\times2=24$ complex amplitudes. However, by virtue of parity invariance relation,

$$\begin{aligned}&\langle\mathbf{q};\lambda_\phi,\lambda_f|T|\mathbf{k};\lambda_\gamma,\lambda_i\rangle\\&\quad=(-1)^{\Lambda_f-\Lambda_i}\langle\mathbf{q};-\lambda_\phi,-\lambda_f|T|\mathbf{k};-\lambda_\gamma,-\lambda_i\rangle,\end{aligned} \tag{2.3}$$

with $\Lambda_f=\lambda_\phi-\lambda_f$ and $\Lambda_i=\lambda_\gamma-\lambda_i$, only 12 complex helicity amplitudes are independent. We label them as [41]

$$\begin{aligned}H_{1,\lambda_\phi}&\equiv\langle\lambda_\phi,\lambda_f=+\tfrac12|T|\lambda_\gamma=1,\lambda_i=-\tfrac12\rangle,\\H_{2,\lambda_\phi}&\equiv\langle\lambda_\phi,\lambda_f=+\tfrac12|T|\lambda_\gamma=1,\lambda_i=+\tfrac12\rangle,\\H_{3,\lambda_\phi}&\equiv\langle\lambda_\phi,\lambda_f=-\tfrac12|T|\lambda_\gamma=1,\lambda_i=-\tfrac12\rangle,\\H_{4,\lambda_\phi}&\equiv\langle\lambda_\phi,\lambda_f=-\tfrac12|T|\lambda_\gamma=1,\lambda_i=+\tfrac12\rangle.\end{aligned} \tag{2.4}$$

The ϕ-meson photoproduction amplitude can then be represented by a 6×4 matrix $\mathcal{F}$ in helicity space:

$$\mathcal{F}\equiv\begin{pmatrix}H_{2,1}&H_{1,1}&H_{3,-1}&-H_{4,-1}\\H_{4,1}&H_{3,1}&-H_{1,-1}&H_{2,-1}\\H_{2,0}&H_{1,0}&-H_{3,0}&H_{4,0}\\H_{4,0}&H_{3,0}&H_{1,0}&-H_{2,0}\\H_{2,-1}&H_{1,-1}&H_{3,1}&-H_{4,1}\\H_{4,-1}&H_{3,-1}&-H_{1,1}&H_{2,1}\end{pmatrix}. \tag{2.5}$$

In actual calculations, sometimes it is easier to evaluate the matrix elements in the nucleon spin space. They are related to the helicity amplitude discussed above, in the reference frame of Fig. 2, by

$$H_{\lambda_\phi,\lambda_f;\lambda_\gamma,\lambda_i}=(-1)^{1-\lambda_i-\lambda_f}\sum_{m_i,m_f} d^{(1/2)}_{m_i,-\lambda_i}(0)d^{(1/2)}_{m_f,-\lambda_f}(\theta) \times\langle\lambda_\phi,m_f|T|\lambda_\gamma,m_i\rangle. \quad (2.6)$$

This expression reduces to that of Ref. [44] for the pseudoscalar meson photoproduction process.

The differential cross section is given by the classical ensemble average as

$$\frac{d\sigma}{d\Omega}=\rho_0\mathrm{Tr}(\rho_F). \quad (2.7)$$

The final state density matrix is

$$\rho_F=\mathcal{F}\rho_I\mathcal{F}^\dagger, \quad (2.8)$$

where ρ_I is the initial state density matrix,

$$\rho_I=\rho_\gamma\rho_N. \quad (2.9)$$

The photon and proton density matrices, ρ_γ and ρ_N, are defined in Appendix A. For example, in the unpolarized case where $\rho_\gamma=\rho_N=\frac{1}{2}$, we get

$$\frac{d\sigma}{d\Omega}^{(U)}=\frac{\rho_0}{4}\mathrm{Tr}(\mathcal{F}\mathcal{F}^\dagger)\equiv\rho_0\mathcal{I}(\theta), \quad (2.10)$$

which defines the cross section intensity $\mathcal{I}(\theta)$.

In general, any spin observable $\overline{\Omega}$ can be written as

$$\overline{\Omega}=\frac{\mathrm{Tr}[\mathcal{F}A_\gamma A_N\mathcal{F}^\dagger B_V B_{N'}]}{\mathrm{Tr}\,(\mathcal{F}\mathcal{F}^\dagger)}, \quad (2.11)$$

where A_N denotes $(\mathbf{1}_2,\boldsymbol{\sigma}_N)$, which are elements of the nucleon density matrix. The explicit forms of A_γ, $B_{N'}$, and B_V can be obtained from the density matrices given in Appendix A. Note that the dimensions of the matrices are $\mathcal{F}(6\times4)$, $A_\gamma A_N(4\times4)$, $\mathcal{F}^\dagger(4\times6)$, and $B_V B_{N'}(6\times6)$.

A. Single polarization observables

When only the incoming photon beam is polarized, we can define the polarized beam asymmetry (analyzing power) Σ_x as

$$\Sigma_x=\frac{\mathrm{Tr}[\mathcal{F}\sigma^x_\gamma\mathcal{F}^\dagger]}{\mathrm{Tr}(\mathcal{F}\mathcal{F}^\dagger)}. \quad (2.12)$$

If we define $\sigma^{(B,T;R,V)}$ for the cross section $d\sigma/d\Omega$ where the superscripts $(B,T;R,V)$ denote the polarizations of (photon beam, target proton; recoil proton, produced vector-meson), then the physical meaning of Σ_x becomes clear through the relation

$$\Sigma_x=\frac{\sigma^{(\|,U;U,U)}-\sigma^{(\perp,U;U,U)}}{\sigma^{(\|,U;U,U)}+\sigma^{(\perp,U;U,U)}}, \quad (2.13)$$

where the superscript U refers to an unpolarized particle and $\|$ $(\perp)$ corresponds to a photon linearly polarized along the $\hat{\mathbf{x}}$ $(\hat{\mathbf{y}})$ axis.

Similarly, we can define the polarized target asymmetry T, recoil polarization asymmetry P, and the vector-meson polarization asymmetry V as

$$T_y=\frac{\mathrm{Tr}(\mathcal{F}\sigma^y_N\mathcal{F}^\dagger)}{\mathrm{Tr}(\mathcal{F}\mathcal{F}^\dagger)},$$

$$P_{y'}=\frac{\mathrm{Tr}(\mathcal{F}\mathcal{F}^\dagger\sigma^{y'}_{N'})}{\mathrm{Tr}(\mathcal{F}\mathcal{F}^\dagger)},$$

$$V_j=\frac{\mathrm{Tr}(\mathcal{F}\mathcal{F}^\dagger\Omega^V_j)}{\mathrm{Tr}(\mathcal{F}\mathcal{F}^\dagger)}, \quad (2.14)$$

where Ω^V_j's are given in Appendix A. The explicit expressions for the single polarization observables can be found in Appendix B.

B. Double polarization observables

There are six double polarization observables: beam-target (BT), beam-recoil (BR), target-recoil (TR), beam–vector-meson (BV), target–vector-meson (TV), and recoil–vector-meson (RV). For example, we define the double polarization observables C^{BT}_{ij} as[1]

$$C^{\mathrm{BT}}_{ij}=\frac{\mathrm{Tr}[\mathcal{F}\sigma^i_\gamma\sigma^j_N\mathcal{F}^\dagger]}{\mathrm{Tr}(\mathcal{F}\mathcal{F}^\dagger)}. \quad (2.15)$$

The physical meaning of C^{BT}_{zz} is then

$$C^{\mathrm{BT}}_{zz}=\frac{\mathrm{Tr}[\mathcal{F}\sigma^z_\gamma\sigma^z_N\mathcal{F}^\dagger]}{\mathrm{Tr}(\mathcal{F}\mathcal{F}^\dagger)} =\frac{\sigma^{(r,z;U,U)}-\sigma^{(r,-z;U,U)}}{\sigma^{(r,z;U,U)}+\sigma^{(r,-z;U,U)}}, \quad (2.16)$$

where the superscript r corresponds to a circularly polarized photon beam with helicity $+1$, and $\pm z$ denotes the direction of the target proton polarization. Some of the double polarization observables are explicitly given in terms of helicity amplitudes in Appendix B. The complete list of double polarization observables can be found in, e.g., Ref. [41].

Among the 290 possible (single, double, triple, and quadruple) polarization observables, we will consider only a few of them including longitudinal asymmetries.[2] For instance, we will not consider the ϕ meson tensor polarization in the double polarization observables throughout this paper.

---

[1]Our definitions of C_{ij} are slightly different from those of Ref. [44]. Our C_{ij} corresponds to C_{ji} of Ref. [44].

[2]We treat the cross section as a single polarization observable. Although there are altogether 290 observables, only 24 of them are linearly independent [41].

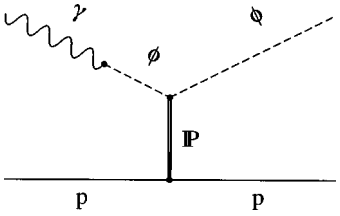

FIG. 3. Diffractive ϕ meson production within the vector-meson-dominance model through Pomeron exchange.

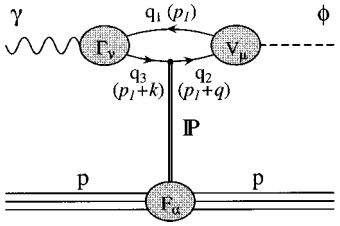

FIG. 4. Quark picture for the Pomeron exchange model of ϕ photoproduction. The four-momenta of the quarks $q_{1,2,3}$ are given in parentheses.

III. THE MODEL FOR ϕ MESON PHOTOPRODUCTION

To calculate the spin observables defined in the last section, we need to construct a model for the helicity amplitudes of ϕ photoproduction. Our model includes the diffractive and OPE production processes and the direct knockout of an $s\bar{s}$ (or uud) cluster in the proton. We describe below the essential dynamics of each process and give the resulting amplitude.

A. Diffractive production

In the VDM diffractive photoproduction [45,46], the incoming photon first converts into vector mesons, i.e., the ϕ-meson in our case, and then this vector meson scatters diffractively from the nucleon through Pomeron exchange, as shown in Fig. 3. Experimental observations for vector-meson production, small-$|t|$ elastic scattering, and diffractive dissociation indicate that Pomeron behaves rather like a $C=+1$ isoscalar photon [47,48]. A microscopic model for vector-meson photo- and electro-production at high energy based on the Pomeron-photon analogy has been proposed by Donnachie and Landshoff [49], and the Pomeron could be successfully described in terms of a nonperturbative two-gluon exchange model [31,50–54].

In our previous calculation [33], we used the vector-meson dominance model with Pomeron-photon analogy within the hadron-Pomeron interaction picture, which is expected to be valid in the low energy region. In this paper, we employ a microscopic model for the VDM. In this approach, the incoming photon first converts into a quark and antiquark pair, which then exchanges a Pomeron[3] with one of the quarks in the proton before recombining into an outgoing ϕ meson, as depicted in Fig. 4. (See, e.g., Ref. [48].) In terms of ϕ (photon) polarization vector ε_ϕ (ε_γ), the invariant amplitude of the diffractive production can be written as

$$T_{fi}^{\mathrm{VDM}}=iT_0\varepsilon_{\phi\mu}^{*}\mathcal{M}^{\mu\nu}\varepsilon_{\gamma\nu}, \tag{3.1}$$

with

$$\mathcal{M}^{\mu\nu}=\mathcal{F}_\alpha\Gamma^{\alpha,\mu\nu}, \tag{3.2}$$

where $\mathcal{F}_\alpha$ describes the Pomeron-nucleon vertex and $\Gamma^{\alpha,\mu\nu}$ is associated with the Pomeron–vector-meson coupling which is related to the $\gamma\to q\bar{q}$ vertex Γ_ν and the $q\bar{q}\to\phi$ vertex V_μ, as shown in Fig. 4. The dynamics of the Pomeron-hadron interactions is contained in T_0.

To determine the explicit forms of the vertices, we have to rely on some model assumptions. Based on the Pomeron-photon analogy, the quark-quark-Pomeron vertex, i.e., $q_2q_3\mathbb{P}$ vertex in Fig. 4, is assumed to be γ_μ. Accordingly, we also have

$$\mathcal{F}_\alpha=\bar{u}(p')\gamma_\alpha u(p), \tag{3.3}$$

where $u(p)$ is the Dirac spinor of the proton with momentum p. The factor N_q of the number of quarks in the proton can be absorbed into T_0.

With the assumptions used in Ref. [48], namely, (i) quarks q_1 and q_2 which recombine into a ϕ-meson are almost on-shell and share equally the four-momentum of the outgoing ϕ, i.e., the nonrelativistic wave function assumption, (ii) quark q_3, which is between photon and Pomeron, is far off-shell, and (iii) $\Gamma_\nu\propto\gamma_\nu$ and $V_\mu\propto\gamma_\mu$, the loop integral in Fig. 4 can be easily carried out to give

$$\bar{\Gamma}^{\alpha,\mu\nu}\propto 2\,\mathrm{Tr}\{\gamma^\mu(\not{p}_1+M_s)\gamma^\nu(\not{p}_1+\not{k}+M_s)\gamma^\alpha(\not{p}_1+\not{q}+M_s)\}, \tag{3.4}$$

where M_s is the s quark mass and p_1 is the 4-momentum of the quark q_1. Explicit calculation leads to

$$\bar{\Gamma}^{\alpha,\mu\nu}=2k^\alpha g^{\mu\nu}-\frac{2}{q^2}k^\alpha q^\mu q^\nu-2g^{\alpha\nu}\left(k^\mu-q^\mu\frac{k\cdot q}{q^2}\right)+2(k^\nu-q^\nu)\left(g^{\mu\alpha}-\frac{q^\alpha q^\mu}{q^2}\right). \tag{3.5}$$

Inspection of Eq. (3.5), however, shows that the last term breaks the gauge invariance[4] so that $\mathcal{M}^{\mu\nu}k_\nu\neq 0$. This arises from the simple assumption about Γ_ν and a more realistic modification of Γ_ν is needed to fix this problem [48]. To have a gauge invariant amplitude, here we simply remove the gauge noninvariant terms by multiplying the projection operator $\mathcal{P}_{\mu\nu}$ from both the left- and right-hand sides of $\bar{\Gamma}^{\alpha,\mu\nu}$ [56], i.e.,

[3]We do not consider the two-gluon-exchange model for the Pomeron in this work.

[4]This problem has also been discussed in Refs. [48,55]. To cure this problem, it was suggested that the quark-gluon structure of the Pomeron in QCD be described in a consistent way [55], or the correct off-shell structure of the electromagnetic interaction of the dressed quarks be taken into account in constituent quark models [48]. However, further detailed discussion on this topic is beyond the scope of this work.

$$\bar{\Gamma}^{\alpha,\mu\nu}\rightarrow\Gamma^{\alpha,\mu\nu}=\mathcal{P}^{\mu\mu'}\bar{\Gamma}^{\alpha}_{\mu'\nu'}\mathcal{P}^{\nu'\nu}, \tag{3.6}$$

where

$$\mathcal{P}_{\mu\nu}=g_{\mu\nu}-\frac{1}{k\cdot q}k_\mu q_\nu. \tag{3.7}$$

It leads to a modified $\Gamma^{\alpha,\mu\nu}$ as

$$\begin{aligned}\Gamma^{\alpha,\mu\nu}=&(k+q)^\alpha g^{\mu\nu}-2k^\mu g^{\alpha\nu}\\&+2\left[k^\nu g^{\alpha\mu}+\frac{q^\mu}{q^2}(k\cdot q g^{\alpha\nu}-k^\alpha q^\nu-q^\alpha k^\nu)\right.\\&\left.-\frac{k^2q^\nu}{q^2k\cdot q}(q^2g^{\alpha\mu}-q^\alpha q^\mu)\right]+(k-q)^\alpha g^{\mu\nu}.\end{aligned} \tag{3.8}$$

Note that although the third term within the square brackets in Eq. (3.8) is essential to ensure the gauge invariance it does not play any role in ϕ photoproduction because $q\cdot\varepsilon_\phi=k\cdot\varepsilon_\gamma=0$ and $k^2=0$ in photoproduction. The last term also does not contribute because $\mathcal{F}\cdot k=\mathcal{F}\cdot q$. Equation (3.8) completes our prescription for the spin structure of VDM amplitude. This should be compared with the $\tilde{\Gamma}^{\alpha,\mu\nu}$ that was used in Ref. [33],

$$\tilde{\Gamma}^{\alpha,\mu\nu}=(k+q)^\alpha g^{\mu\nu}-k^\mu g^{\alpha\nu}-q^\nu g^{\alpha\mu}, \tag{3.9}$$

which was obtained by gauging the massive vector-field Lagrangian in the usual way [57,58] for the $\phi\phi\mathbb{P}$ vertex. Note that $\tilde{\Gamma}^{\alpha,\mu\nu}$ is obtained within the hadron-Pomeron interaction picture while we attempt to use a microscopic quark-Pomeron interaction scheme instead in this paper. Note the similarity between Eqs. (3.8) and (3.9) as well. More detailed discussion on the comparison of $\Gamma^{\alpha,\mu\nu}$ with $\tilde{\Gamma}^{\alpha,\mu\nu}$ is given in Appendix C together with the gauge invariance of $\tilde{\Gamma}^{\alpha,\mu\nu}$.

The factor T_0 in Eq. (3.1) includes the dynamics of the Pomeron-hadron interaction. We use the form and parameters of T_0 determined in Ref. [59], which reads

$$\left(\frac{d\sigma}{dt}\right)_{\rm VDM}=\sigma_\gamma(W)b_\phi\exp(-b_\phi|t-t_{\rm max}|), \tag{3.10}$$

with $b_\phi=4.01$ GeV^{-2} and $\sigma_\gamma(W)=0.2$ μb around $W=2\sim3$ GeV.[5] This normalizes the amplitude T_0 and explicitly we have

$$T_0=\frac{W^2-M_N^2}{M_N\mathcal{N}}\sqrt{4\pi\sigma_\gamma(W)b_\phi}\exp(-\tfrac{1}{2}b_\phi|t-t_{\rm max}|), \tag{3.11}$$

where

$$t_{\rm max}=|t|_{\rm min}=2M_N^2-2E_pE_{p'}+2|\mathbf{k}||\mathbf{q}|, \tag{3.12}$$

and the normalization constant $\mathcal{N}$ reads

$$\begin{aligned}\mathcal{N}^2=&\frac{2}{M_N^2M_\phi^2}\{k\cdot p[k\cdot pM_\phi^2+(k\cdot q)^2]\\&+2k\cdot pk\cdot q[p\cdot q-2M_\phi^2]-(k\cdot q)^2[p\cdot q+M_N^2]\}.\end{aligned} \tag{3.13}$$

It is now straightforward to obtain the VDM helicity amplitude as

$$H^{\rm VDM}_{\lambda_\phi,\lambda_f;\lambda_\gamma,\lambda_i}=\sum_{m_i,m_f}d^{(1/2)}_{m_f,\lambda_f}(\pi+\theta)d^{(1/2)}_{m_i,\lambda_i}(\pi)T^{\rm VDM}_{\lambda_\phi,m_f;\lambda_\gamma,m_i}, \tag{3.14}$$

where

$$\begin{aligned}&T^{\rm VDM}_{\lambda_\phi,m_f;\lambda_\gamma,m_i}\\&=iCT_0\left\{[(1+\alpha\alpha'\cos\theta)(\mathcal{V}^0-\mathcal{W}^0)-a^z(\mathcal{V}^z-\mathcal{W}^z)\right.\\&\quad+a^x\mathcal{W}^x-2m_ib^x\,\mathrm{Im}\,\mathcal{W}^y]\delta_{m_im_f}\\&\quad+2m_i\left[\alpha\alpha'\sin\theta(\mathcal{V}^0-\mathcal{W}^0)-b^x(\mathcal{V}^z-\mathcal{W}^z)-b^z\mathcal{W}^x\right.\\&\quad\left.\left.+\frac{1}{2m_i}b^z\mathrm{Im}\,\mathcal{W}^y\right]\delta_{m_i,-m_f}\right\},\end{aligned} \tag{3.15}$$

with $C=\sqrt{(\gamma_p+1)(\gamma_p'+1)}/2$ and θ is the c.m. scattering angle. Definitions for the other variables and their detailed derivation are given in Appendix D. Close inspection of this amplitude shows that at small $|t|$ (or $\theta\rightarrow0$), the dominant part, namely the $(k+q)^\alpha g^{\mu\nu}$ term in $\Gamma^{\alpha,\mu\nu}$, has the spin/helicity conserving form as known in the conventional VDM amplitude,

$$\begin{aligned}T^{\rm VDM}_{\lambda_\phi,m_f;\lambda_\gamma,m_i}&\simeq-2i|\mathbf{k}|CT_0(1+\alpha\alpha')\delta_{\lambda_\phi\lambda_\gamma}\\&\equiv-iM_0^{\rm VDM}\delta_{\lambda_\phi\lambda_\gamma}\delta_{m_im_f},\end{aligned} \tag{3.16}$$

while the spin-flip part is suppressed. Note also that $T^{\rm VDM}$ is purely imaginary.

B. One-pion-exchange in ϕ photoproduction

At low photon energy, a one-pion-exchange diagram (Fig. 5) gives non-negligible contribution. This may be regarded as a correction to the VDM process [37].

The effective Lagrangian for the $\phi\gamma\pi$ interaction has the form

$$\mathcal{L}_{\phi\gamma\pi}=\tilde{g}_{\phi\gamma\pi}\epsilon^{\mu\nu\alpha\beta}\partial_\mu\phi_\nu\partial_\alpha A_\beta\pi^0, \tag{3.17}$$

[5]There are two comments concerning the parameters. First, these parameters may be dependent on the energy scale. However, for our present qualitative study we will assume constant values for them at $W=2\sim3$ GeV throughout this paper. Second, the parameters are determined by fitting the formula (3.10) to the experimental data, so the contributions from the knockout and OPE processes are neglected. However, as we will see, these mechanisms of the ϕ photoproduction are suppressed compared with that of the VDM and the use of this parameter set is justified.

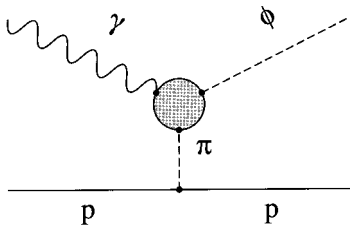

FIG. 5. One-pion-exchange process in ϕ photoproduction.

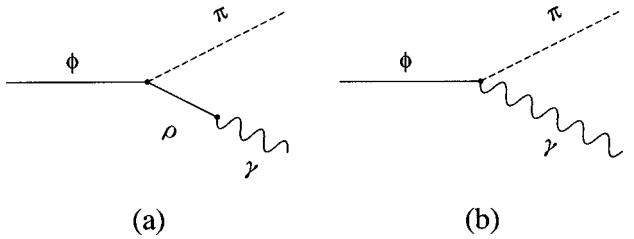

FIG. 6. Two possible mechanisms of $\phi\to\gamma\pi$ decay.

where A_β is the photon field. The effective coupling constant $\tilde{g}_{\phi\gamma\pi}$ can be estimated through the decay width of $\phi\to\gamma\pi$, which reads

$$\Gamma(\phi\to\gamma\pi)=\frac{1}{96\pi}\frac{(M_\phi^2-M_\pi^2)^3}{M_\phi^3}\tilde{g}_{\phi\gamma\pi}^2. \tag{3.18}$$

From the empirical value of $\Gamma(\phi\to\gamma\pi^0)=5.8\times10^{-6}$ GeV, we get $\tilde{g}_{\phi\gamma\pi}=0.042$ GeV^{-1}. A remark is needed here concerning this estimate. The blob in Fig. 5 contains two processes as shown in Fig. 6. In addition to the VDM-like process of Fig. 6(a), there is another Gell-Mann–Sharp–Wagner type diagram shown in Fig. 6(b). In the pure VDM, the decay process is completely dominated by Fig. 6(a) and there is no contact term. However, this pure VDM diagram gives

$$\Gamma(\phi\to\gamma\pi)_{\rm VDM}=\frac{\alpha_e}{24}\frac{g_{\phi\rho\pi}^2(M_\phi^2-M_\pi^2)^3}{M_\phi^3 f_\rho^2}=1.65\times10^{-5}\ \text{GeV}, \tag{3.19}$$

with the ρ-meson decay constant f_ρ $(=5.04)$, $\alpha_e=e^2/4\pi$, and $g_{\phi\rho\pi}=1.19$ GeV^{-1}. Thus the pure VDM overestimates the decay width by a factor of 3 and we have to allow for the contact term of Fig. 6(b) to fit the experimental decay width. However, since the two transition amplitudes of Fig. 6 have the same structure, we combine the two processes into one term as in Eq. (3.17) with an effective coupling constant $\tilde{g}_{\phi\gamma\pi}$.

For the $NN\pi$ interaction, one can use either pseudoscalar or pseudovector coupling, which are equivalent at the tree level. For definiteness we use the pseudoscalar coupling of the form

$$\mathcal{L}_{PS}=-ig_{\pi NN}\bar{N}\gamma_5\boldsymbol{\tau}\cdot\boldsymbol{\pi}N, \tag{3.20}$$

with $g_{\pi NN}^2/4\pi=14.3$.

To include the off-shell effects, each vertex in Fig. 5 has to be modified with a form factor. We follow Ref. [37] and use the Benecke-Dürr form factors [60] in which the πNN form factor F_N and the $\phi\gamma\pi$ form factor F_ϕ are parametrized as

$$F_N=\frac{1+(2.9)^2Q_N^2}{1+(2.9)^2Q_{NT}^2},\quad F_\phi=\frac{U(2.3Q_F)}{U(2.3Q_T)}\left(\frac{Q_T}{Q_F}\right)^2, \tag{3.21}$$

where Q_N (Q_{NT}) is the on-shell (off-shell) π-N c.m. momentum and Q_T (Q_F) is the momentum of the on-shell (off-shell) pion in the ϕ rest frame [61], respectively,

$$Q_N^2=\frac{M_\pi^2(M_\pi^2-4M_N^2)}{4M_N^2},\quad Q_{NT}^2=\frac{t(t-4M_N^2)}{4M_N^2},$$

$$Q_T=\frac{1}{2M_\phi}(M_\phi^2-M_\pi^2),\quad Q_F=\frac{1}{2M_\phi}(M_\phi^2-t). \tag{3.22}$$

$U(x)$ is given as

$$U(x)=\frac{1}{2x^2}\left[\frac{2x^2+1}{4x^2}\log(4x^2+1)-1\right]. \tag{3.23}$$

Before using these form factors, one should be careful with the use of factor 2.3 in F_ϕ of Eq. (3.21) since this factor is determined for the $\omega\gamma\pi$ coupling [37]. However, since we do not have enough data for the ϕ meson case, we will use this value in our qualitative study on ϕ photoproduction.

The T matrix element of the OPE process then reads

$$T_{fi}^{\rm OPE}=\frac{i}{t-M_\pi^2}g_{NN\pi}\tilde{g}_{\phi\gamma\pi}W^F_{m_f,m_i}W^B_{\lambda_\phi,\lambda_\gamma}, \tag{3.24}$$

where the coupling constants contain the Benecke-Dürr form factors and

$$W^F_{m_f,m_i}=\bar{u}(p')\gamma_5u(p),\quad W^B_{\lambda_\phi,\lambda_\gamma}=\epsilon^{\mu\nu\alpha\beta}q_\mu k_\alpha\varepsilon_{\phi\nu}\varepsilon_{\gamma\beta}. \tag{3.25}$$

Direct calculation of W^F and W^B gives

$$W^F_{m_f,m_i}=C[2m_f(\alpha'\cos\theta-\alpha)\delta_{m_fm_i}-\alpha'\sin\theta\delta_{m_f-m_i}],$$

$$W^B_{\lambda_\phi,\lambda_\gamma}=iE_\gamma\left[\lambda_\gamma(E_\phi-|\mathbf{q}|\cos\theta)\boldsymbol{\varepsilon}_\phi\cdot\boldsymbol{\varepsilon}_\gamma+\frac{|\mathbf{q}|\sin\theta}{\sqrt{2}M_\phi}(|\mathbf{q}|-|\mathbf{q}|E_\phi\cos\theta)\delta_{\lambda_\phi0}-\frac{\lambda_\phi|\mathbf{q}|\sin^2\theta}{2}\right], \tag{3.26}$$

where

$$\boldsymbol{\varepsilon}_\phi\cdot\boldsymbol{\varepsilon}_\gamma=\left[1+\left(\frac{E_\phi}{M_\phi}-1\right)\delta_{\lambda_\phi0}\right]d^{(1)}_{\lambda_\gamma,\lambda\phi}(\theta), \tag{3.27}$$

and α and α' are given in Appendix D. Note also that the OPE amplitude is purely real. This implies that it does not

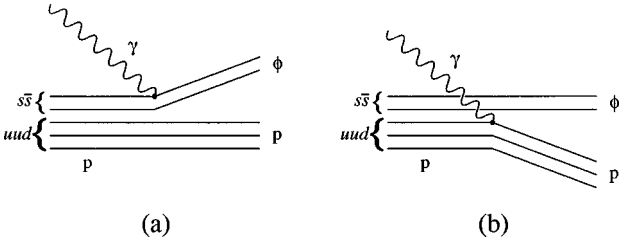

FIG. 7. (a) $s\bar{s}$-knockout and (b) uud-knockout contributions to ϕ meson photoproduction.

interfere with the knockout amplitudes in the differential cross section as we shall see below.

One may also consider the t-channel η-meson exchange instead of pion. In fact, the decay width of $\phi\to\gamma\eta$ is about 5.58×10^{-5} GeV, which is larger than $\Gamma(\phi\to\gamma\pi)$ by an order of magnitude. This gives us the large $\phi\gamma\eta$ coupling constant $g_{\phi\gamma\eta}=0.218$ GeV^{-1} as compared to $g_{\phi\gamma\pi}=0.042$ GeV^{-1}. However, we should also consider the ηNN coupling. By assuming SU(3) flavor symmetry, one obtains $g_{\eta NN}/g_{\pi^0 NN}=(1/\sqrt{3})\cdot(D-3F)/(D+F)\simeq-0.19\sim-0.35$ using $F/D=0.5\sim2/3$, and we find that the product of the coupling constants in the η-exchange diagram is of the same order of magnitude as that of OPE. Nevertheless, because of its heavier mass, the η-meson exchange amplitude is expected to be smaller than that of OPE at least in the forward scattering region. There can also be cancellation between the two because $g_{\eta NN}/g_{\pi^0 NN}<0$. In this work, therefore, we will not consider the η-meson exchange diagram in ϕ photoproduction.[6]

C. Direct knockout production

When the incoming photon interacts with the five-quark component of the proton, we have an additional process called direct knockout as shown in Fig. 7. This process can be classified, according to the struck quark cluster, into $s\bar{s}$- and uud-knockout. In order to investigate the effects from the hidden strangeness content of the proton in ϕ photoproduction, we parametrize the proton wave function in Fock space as

$$|p\rangle=A_0|uud\rangle+\sum_X A_X|uudX\rangle+\sum_X B_X|uuds\bar{s}X\rangle, \tag{3.28}$$

where X denotes any combination of gluons and light quark pairs of u and d quarks. Our aim is to estimate $|B_X|^2$ by isolating the OZI evasion processes. Ellis *et al.* [22] estimated it to be 1–19 % from an analysis of $p\bar{p}$ annihilation. From the ϕ electroproduction process, Henley *et al.* [27] claimed that its theoretical upper bound would be 10–20 %. We improved their prediction by employing a relativistic quark model [29,30], and showed that the upper bound could be lowered to 3–5 %.

[6]Furthermore, since this one-boson-exchange amplitude is purely real, its contribution to the double polarization observables is expected to be negligible. See Eq. (4.10).

For simplicity and for our qualitative study, we approximate the proton wave function (3.28) as

$$|p\rangle=A|uud\rangle+B|uuds\bar{s}\rangle. \tag{3.29}$$

This parametrization of the nucleon wave function can be justified in our case of ϕ production as argued in Refs. [27–30]. To compensate for the negative parity of the $s\bar{s}$ cluster, only the odd orbital excitations in the wave function of relative motion between uud and $s\bar{s}$ clusters are allowed. In principle, there are two more configurations when we consider the first orbital excitation of the quark clusters: either the $s\bar{s}$ cluster or the uud cluster is orbitally excited. In this section, we consider only the $s\bar{s}$ clusters with $j^P_{s\bar{s}}=0^-$ and 1^-, where $j^P_{s\bar{s}}$ stands for the spin of an $s\bar{s}$ cluster of parity P, and leave the study of the other quark-cluster configurations to Sec. V. The proton wave function can then be expressed as

$$|p\rangle=A|[uud]^{1/2}\rangle+\sum_{j_{s\bar{s}}=0,1;j_c} b_{j_{s\bar{s}}}|[[[uud]^{1/2}\otimes[\mathbf{L}]]^{j_c}\otimes[s\bar{s}]^{j_{s\bar{s}}}]^{1/2}\rangle, \tag{3.30}$$

where the superscripts 1/2 and $j_{s\bar{s}}$ denote the spin of each cluster and (b_0,b_1) correspond to the amplitudes of the $s\bar{s}$ cluster with spin 0 and 1, respectively. The strangeness admixture of the proton, B^2, is then defined to be $\Sigma|b_{j_{s\bar{s}}}|^2$, which is constrained to $A^2+B^2=1$ by the normalization of the wave function. The symbol $\otimes$ represents vector addition of the cluster spins and the orbital angular momentum $\mathbf{L}$. We choose the lowest negative-parity excitation with $\ell=1$. For $j_{s\bar{s}}=1$, j_c ($\mathbf{J}_c=\mathbf{S}_{uud}+\mathbf{L}$) can either be 1/2 or 3/2 because $s_{uud}=1/2$ and $\ell=1$. As in Ref. [30], we assume that the two possible states have the same amplitude. We also limit our consideration to color-singlet cluster configurations, assuming that hidden color configurations do not contribute to the single (one-step) knockout processes [27,30]. Our analyses show that the different $s\bar{s}$ configurations play different roles in the knockout production.

When the incoming photon strikes the $s\bar{s}$ cluster, we have the $s\bar{s}$-knockout process as shown in Fig. 7(a), and Fig. 7(b) corresponds to the uud knockout. In the $s\bar{s}$-knockout process, the symmetry property of the spatial wave functions in the initial proton state only allows for the magnetic transition to contribute, while electric (spin-independent) transition is forbidden. Then the transition amplitude is proportional to the matrix element

$$\langle S_\phi=1|\boldsymbol{\sigma}_s-\boldsymbol{\sigma}_{\bar{s}}|j_{\bar{s}s}=0,1\rangle\cdot(\mathbf{q}\times\boldsymbol{\varepsilon}_\gamma), \tag{3.31}$$

so that only the antisymmetric initial state with $j_{s\bar{s}}=0$ contributes. This leads to $T^{s\bar{s}}_{fi}\propto b_0$. In the case of uud knockout, the $s\bar{s}$ cluster is a spectator, and only $j_{\bar{s}s}=1$ state can match the physical outgoing ϕ meson. Here, both the electric and magnetic transitions contribute and $T^{uud}_{fi}\propto b_1$.

The detailed description of the knockout process with the relativistic harmonic oscillator quark model and its electromagnetic current can be found in Refs. [29,30]. In this paper we just quote the relevant results. The knockout amplitudes

are most easily evaluated in the laboratory frame as given in Ref. [30]. After transforming into the c.m. frame, they read

$$T^{s\bar{s}}_{m_\phi,m_f;\lambda_\gamma,m_i}=iT_0^{s\bar{s}}\mathcal{S}^{s\bar{s}}_{m_\phi,m_f;\lambda_\gamma,m_i},$$

$$T^{uud}_{m_\phi,m_f;\lambda_\gamma,m_i}=iT_0^{uud}\mathcal{S}^{uud}_{m_\phi,m_f;\lambda_\gamma,m_i}. \tag{3.32}$$

Here $T_0^{s\bar{s}}$ and T_0^{uud} include the dependence of the amplitudes on the energy and momentum transfer, and $\mathcal{S}^{s\bar{s}}$ and $\mathcal{S}^{uud}$ contain their spin structure. Explicitly they take the form,

$$T_0^{s\bar{s}}=\left(\frac{8\pi\alpha_e E_\phi^L E_{p'}^L}{M_N}\right)^{1/2} A^* b_0 F_{s\bar{s}}(\gamma_\phi^L,q_{s\bar{s}})$$
$$\times F_{uud}(\gamma_{p'}^L,0)V_{s\bar{s}}(\mathbf{p}'_L)\frac{\mu_s E_\gamma^L}{3M_N},$$

$$T_0^{uud}=\left(\frac{8\pi\alpha_e E_\phi^L E_{p'}^L}{M_N}\right)^{1/2} A^* b_1 F_{s\bar{s}}(\gamma_\phi^L,0)$$
$$\times F_{uud}(\gamma_{p'}^L,q_{uud})V_{uud}(\mathbf{q}_L)\frac{\mu E_\gamma^L}{2M_N}, \tag{3.33}$$

and

$$\mathcal{S}^{s\bar{s}}_{fi}=\sqrt{3}\sum_\varrho \langle \tfrac{1}{2}m_f 1\varrho|\tfrac{1}{2}m_i\rangle \xi^{s\bar{s}}_\varrho \lambda_\gamma \boldsymbol{\varepsilon}^*_\phi(m_\phi)\cdot\boldsymbol{\varepsilon}_\gamma(\lambda_\gamma),$$

$$\mathcal{S}^{uud}_{fi}=-\sqrt{3}\sum_{\varrho,j_c,m_c}\langle \tfrac{1}{2}m_f-\lambda_\gamma 1\varrho|j_c m_c\rangle$$
$$\times\langle j_c m_c 1 m_\phi|\tfrac{1}{2}m_i\rangle\xi^{uud}_\varrho, \tag{3.34}$$

where

$$\xi^{s\bar{s}}_{\pm1}=\pm\frac{1}{\sqrt{2}}\sin\theta_{p'},\quad \xi^{uud}_{\pm1}=\mp\frac{1}{\sqrt{2}}\sin\theta_q,$$
$$\xi^{s\bar{s}}_0=\cos\theta_{p'},\quad \xi^{uud}_0=\cos\theta_q, \tag{3.35}$$

with θ_α being the production angle in the laboratory frame. In addition, we use $\mu_s=M_N/M_s$, and $\mu=M_N/M_q$, with s quark mass M_s ($=500$ MeV) and u,d quark mass M_q ($=330$ MeV). The functions F_β's ($\beta=s\bar{s},uud$) are the Fourier transforms of the overlap of the spatial wave functions of the struck cluster β in the entrance and exit channels [30], which read

$$F_{s\bar{s}}(\gamma_\phi^L,q_{s\bar{s}})=(\gamma_\phi^L)^{-1}\exp(-r_{s\bar{s}}^2q_{s\bar{s}}^2/6)$$
$$=(\gamma_\phi^L)^{-1}\exp\{-q_{s\bar{s}}^2/(8\Omega_\rho)\},$$

$$F_{uud}(\gamma_{p'}^L,q_{uud})=(\gamma_{p'}^L)^{-2}\exp(-r_{uud}^2q_{uud}^2/6)$$
$$=(\gamma_{p'}^L)^{-2}\exp\{-q_{uud}^2/(6\Omega_\xi)\},$$

$$\gamma_{p'}^L=\frac{E_{p'}^L}{M_N},\quad q_{uud}^2=2(E_\gamma^L)^2-\frac{E_\gamma^L}{E_{p'}^L}[(E_\gamma^L)^2+\mathbf{p}_L'^2-\mathbf{q}_L^2],$$

$$\gamma_\phi^L=\frac{E_\phi^L}{M_\phi},\quad q_{s\bar{s}}^2=2(E_\gamma^L)^2-\frac{E_\gamma^L}{E_{p'}^L}[(E_\gamma^L)^2-\mathbf{p}_L'^2+\mathbf{q}_L^2], \tag{3.37}$$

where r_{uud} and $r_{s\bar{s}}$ are the rms radii of the proton and ϕ meson, respectively, and $\Omega_{\rho,\xi}$ are the harmonic oscillator parameters. We use the parameters determined in Ref. [30] as $\sqrt{\Omega_\xi}=1.89$ fm^{-1} and $\sqrt{\Omega_\rho}=3.02$ fm^{-1}.

The momentum distribution function $V_\beta(p)$ of cluster β is given by

$$\frac{1}{(2\pi)^3}V_\beta(\mathbf{p})=\frac{v_\beta(\mathbf{p})}{\int d\mathbf{p}v_\beta(\mathbf{p})},$$

$$v_\beta(\mathbf{p})=\mathbf{p}^2\exp\left\{-\frac{5}{3\Omega_\chi}(\mathbf{p}^2-x_\beta M_N E_\beta)\right\}, \tag{3.38}$$

where $x_{s\bar{s}}=3/5$, $E_{s\bar{s}}=E_{p'}^L$, and $x_{uud}=2/5$, $E_{uud}=E_\phi^L$. The parameter Ω_χ is again related to the hadron rms radii and taken to be $\sqrt{\Omega_\chi}=2.63$ fm^{-1} [30].

Note that all knockout amplitudes are purely imaginary, which indicates the absorption of incoming photon by the five-quark component of the proton. Therefore, they do not interfere with the OPE amplitude in the differential cross section. However, we do expect a strong interference between the dominant imaginary part of the VDM photoproduction and knockout amplitudes.

IV. RESULTS

It is straightforward, with the help of Eq. (2.6), to obtain the helicity amplitudes of the knockout and OPE processes. The total photoproduction helicity amplitude H is given by

$$H=H^{\rm VDM}+H^{s\bar{s}}+H^{uud}+H^{\rm OPE}. \tag{4.1}$$

We can then proceed to calculate various spin observables with the formulas developed in Sec. II and Appendix B. Among those presented in Appendix B, we focus on those which are found to be strongly dependent on the strangeness content of the proton.

A. Unpolarized cross section

Before studying the spin observables, let us discuss the parameters of our model. In addition to the parameters of the VDM and RHOQM fixed in Sec. III, we have to determine the amplitudes $b_{0,1}$ of the proton wave function (3.30). As we will see, the prediction on the spin observables is sensitive to the combination $A^*b_{j_{s\bar{s}}}\equiv\eta_{j_{s\bar{s}}}|A^*b_{j_{s\bar{s}}}|$, where $\eta_{j_{s\bar{s}}}$ ($=\pm1$) is the relative phase between the strange and nonstrange amplitudes. In principle, the purpose of this study is to determine these values by comparing the predictions with the experimental data. However, because of the lack of ex-

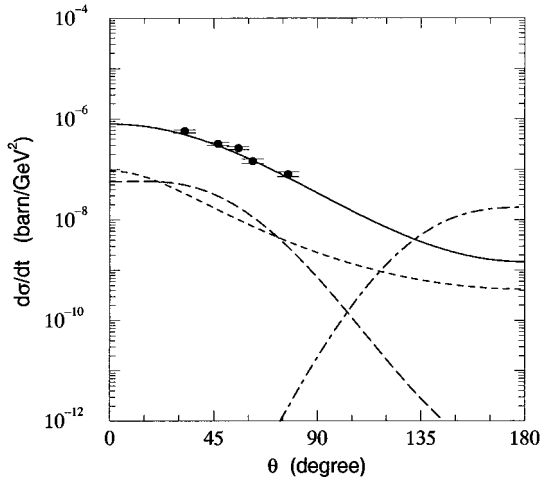

FIG. 8. The unpolarized photoproduction cross section $d\sigma/dt(\theta)$ at $W=2.155$ GeV ($E_\gamma^L=2.0$ GeV). The solid, dotted, dashed, and dot-dashed lines give the cross section of VDM, OPE, $s\bar{s}$ knockout, and uud knockout, respectively, with strangeness admixture $B^2=1\%$ and $|b_0|=|b_1|=B/\sqrt{2}$. The experimental data are from Ref. [59].

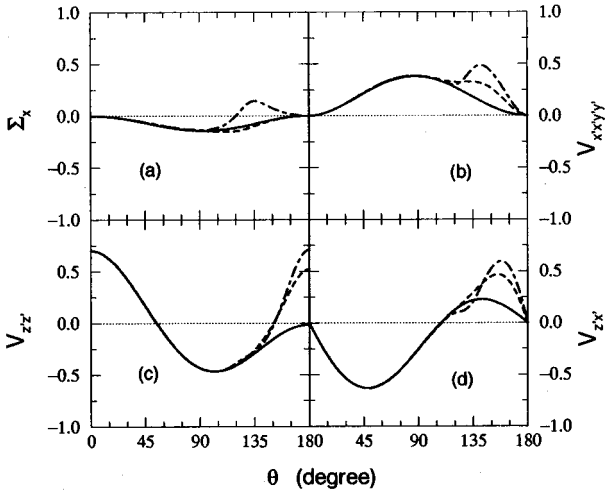

FIG. 9. The single spin observables (a) Σ_x, (b) $V_{x'x'y'y'}$, (c) $V_{z'z'}$, and (d) $V_{z'x'}$ at $W=2.155$ GeV ($E_\gamma^L=2.0$ GeV). The solid lines represent the predictions of VDM plus OPE, i.e., $B^2=0$, and the dashed and dot-dashed lines are for $(\eta_0=+1,\eta_1=+1)$ and $(+1,-1)$ with $B^2=1\%$, respectively. The dependence on η_0 is negligible and the results for $(-1,+1)$ and $(-1,-1)$ are not shown.

perimental data, we will make an assumption about these values and compare our results with the pure VDM and OPE predictions that are associated with the $B^2=0$ case. For simplicity, we assume $b_0^2=b_1^2=B^2/2$.

The result of our numerical calculation on the unpolarized ϕ photoproduction within the RHOQM is shown in Fig. 8. In Ref. [30], we have argued that a theoretical upper bound of B^2 would be around 3–5 %. In Fig. 8, we carry out the calculation with the strangeness probability $B^2=0.01$. We find that the VDM process dominates the knockout and OPE mechanisms except in the backward scattering region. However, our results at large scattering angles should not be taken seriously because, in this region the applicability of the VDM is questionable and the contributions from the intermediate excited hadronic states are expected to be important. Therefore, the VDM gives the dominant contribution to the cross section in the kinematical region at small scattering angles in which we are interested.

B. Polarization observables

We show our predictions for the single polarization asymmetries, Σ_x, $V_{x'x'y'y'}$, $V_{z'z'}$, and $V_{z'x'}$, in Fig. 9. It turns out that the single polarization asymmetries are not sensitive to the strange quark admixture of the proton. However, the story is totally different for the double polarization asymmetries, namely, some of them are very sensitive to the strange admixture in the proton. Before presenting our numerical results for double polarization observables, we first discuss qualitatively why they are important.

Let us consider the most interesting region of t, i.e., $|t|\rightarrow|t|_{\min}$ (or $\theta\rightarrow 0$), where the differential cross section is maximal. Here we can neglect the uud-knockout mechanism because the uud-knockout cross section is suppressed in the forward scattering region. As shown in Eq. (3.16), the diffractive photoproduction amplitude has the following helicity conserving form in this region:

$$H^{\rm VDM}_{\lambda_\phi,\lambda_f;\lambda_\gamma,\lambda_i}\simeq -iM_0^{\rm VDM}\,\delta_{\lambda_f\lambda_i}\delta_{\lambda_\phi\lambda_\gamma}, \tag{4.2}$$

where $M_0^{\rm VDM}$ denotes the corresponding amplitude at $|t|\sim|t|_{\min}$.

For the $s\bar{s}$-knockout amplitude we use $\hat{p}'_\nu\simeq\delta_{\nu 0}$ at $|t|\simeq|t|_{\min}$ and $\langle\frac{1}{2}\lambda_i 10|\frac{1}{2}\lambda_i\rangle=2\lambda_i/\sqrt{3}$ to obtain

$$H^{s\bar{s}}_{\lambda_\phi,\lambda_f;\lambda_\gamma,\lambda_i}\simeq -iM_0^{s\bar{s}}(2\lambda_i\lambda_\gamma)\,\delta_{\lambda_f\lambda_i}\delta_{\lambda_\phi\lambda_\gamma}. \tag{4.3}$$

Comparison of the helicity dependence of Eqs. (4.2) and (4.3) shows that the $s\bar{s}$-knockout helicity conserving amplitude has an additional important phase factor $(2\lambda_i\lambda_\gamma)$. Here, the λ_γ factor comes from the magnetic structure of the electromagnetic interaction while $2\lambda_i$ results from the coupling of $\mathbf{S}_{uud}$ with $\mathbf{L}$ in the initial proton. The OPE amplitude in this region reads

$$H^{\rm OPE}_{\lambda_\phi,\lambda_f;\lambda_\gamma,\lambda_i}\simeq -M_0^{\rm OPE}(2\lambda_i\lambda_\gamma)\,\delta_{\lambda_f\lambda_i}\delta_{\lambda_\phi\lambda_\gamma}. \tag{4.4}$$

Then the total photoproduction amplitude at small θ becomes

$$H_{\lambda_\phi,\lambda_f;\lambda_\gamma,\lambda_i}\simeq[-i(M_0^{\rm VDM}+2\lambda_i\lambda_\gamma M_0^{s\bar{s}}) - 2\lambda_i\lambda_\gamma M_0^{\rm OPE}]\,\delta_{\lambda_f\lambda_i}\delta_{\lambda_\phi\lambda_\gamma}. \tag{4.5}$$

Note that in most calculations the Pomeron exchange amplitude is assumed to be almost imaginary by the optical theorem. In this approximation, the OPE amplitude does not interfere with the rest because all the other amplitudes are purely imaginary. However, the VDM amplitude may have some real part that could interfere with the OPE contribution

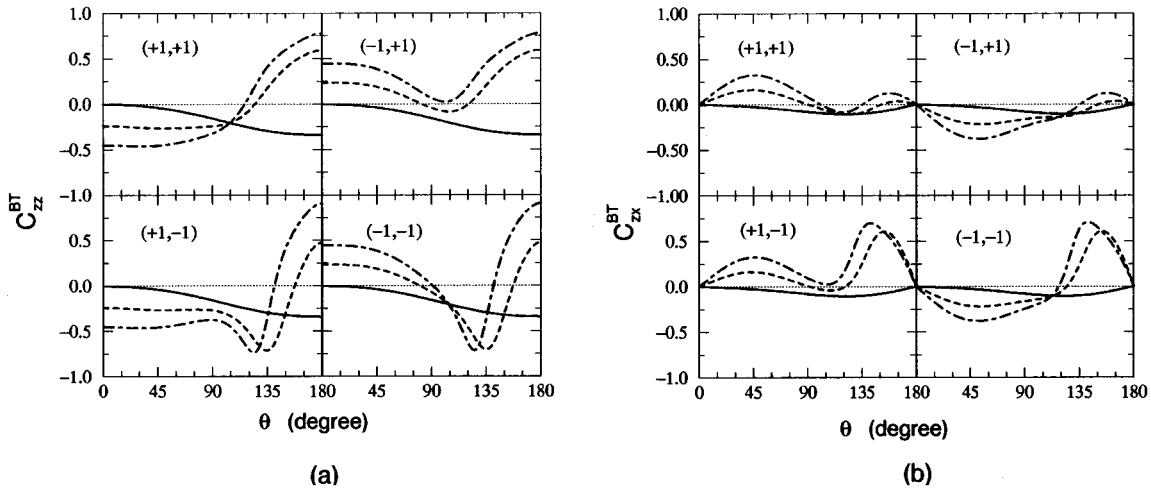

FIG. 10. The double spin asymmetry (a) $C_{zz}^{\mathrm{BT}}(\theta)$ and (b) $C_{zx}^{\mathrm{BT}}(\theta)$ at $W=2.155$ GeV with $B^2=0\%$, i.e., the VDM and OPE (solid lines), 0.25% (dashed lines), and 1% (dot-dashed lines) assuming that $|b_0|=|b_1|$. The phases (η_0,η_1) are explicitly given in each graph.

[62]. One may estimate this part by using the subtracted dispersion relation for the amplitude $f(s,t)$, which is normalized to $s\sigma_T=\mathrm{Im}\, f(s,t_{\max})$ with $s=W^2$ [63],

$$\mathrm{Re}\, f(s,t)=\frac{2s^2}{\pi}\mathrm{P}\int_{s_{\min}}^{\infty}\frac{ds'}{s'(s'^2-s^2)}\mathrm{Im}\, f(s,t). \tag{4.6}$$

In Ref. [63] this integral was evaluated analytically in the limit of high energy. Unfortunately, however, this method cannot be applied to the finite s region and we must evaluate Eq. (4.6) numerically. Assuming the standard s dependence of the imaginary part as $f\sim s^{\alpha_P}$ with $\alpha_P\simeq 1$, we can get the ratio $\xi\equiv\mathrm{Re}\, f(s,t)/\mathrm{Im}\, f(s,t)=0.12\sim 0.086$ at $E_\gamma=2\sim 3$ GeV. Therefore, we are justified to assume the real part of the VDM amplitude as

$$\mathrm{Re}\, H^{\mathrm{VDM}}_{\lambda_\phi,\lambda_f,\lambda_\gamma,\lambda_i,}=-\xi M_0^{\mathrm{VDM}}\delta_{\lambda_f\lambda_i}\delta_{\lambda_\phi\lambda_\gamma}. \tag{4.7}$$

Then the total amplitude reads

$$H_{\lambda_\phi,\lambda_f,\lambda_\gamma,\lambda_i,}\simeq-[i(M_0^{\mathrm{VDM}}+2\lambda_i\lambda_\gamma M_0^{s\bar{s}}) +(\xi M_0^{\mathrm{VDM}}+2\lambda_i\lambda_\gamma M_0^{\mathrm{OPE}})]\delta_{\lambda_f\lambda_i}\delta_{\lambda_\phi\lambda_\gamma}. \tag{4.8}$$

As an example, let us consider the beam-target asymmetry C_{zz}^{BT} for the circularly polarized photon beam. It may be written as

$$C_{zz}^{\mathrm{BT}}=\frac{d\sigma(\frac{1}{2})-d\sigma(\frac{3}{2})}{d\sigma(\frac{1}{2})+d\sigma(\frac{3}{2})}, \tag{4.9}$$

where $d\sigma$ represents $d\sigma/dt$ and $\frac{3}{2}$ and $\frac{1}{2}$ denote the sum of the initial proton and photon helicities. In the former case λ_i and λ_γ have the same sign while in the latter they have opposite signs. Thus we get

$$\begin{aligned}C_{zz}^{\mathrm{BT}}&\simeq\frac{|i(M_0^{\mathrm{VDM}}-M_0^{s\bar{s}})+\xi M_0^{\mathrm{VDM}}-M_0^{\mathrm{OPE}}|^2-|i(M_0^{\mathrm{VDM}}+M_0^{s\bar{s}})+\xi M_0^{\mathrm{VDM}}+M_0^{\mathrm{OPE}}|^2}{|i(M_0^{\mathrm{VDM}}-M_0^{s\bar{s}})+\xi M_0^{\mathrm{VDM}}-M_0^{\mathrm{OPE}}|^2+|i(M_0^{\mathrm{VDM}}+M_0^{s\bar{s}})+\xi M_0^{\mathrm{VDM}}+M_0^{\mathrm{OPE}}|^2}\\&\simeq-2\frac{(M_0^{\mathrm{VDM}}M_0^{s\bar{s}})+\xi M_0^{\mathrm{VDM}}M_0^{\mathrm{OPE}}}{|M_0^{\mathrm{VDM}}|^2}\\&\simeq-2\eta_0\sqrt{\frac{\sigma^{s\bar{s}}}{\sigma^{\mathrm{VDM}}}}-2\xi\sqrt{\frac{\sigma^{\mathrm{OPE}}}{\sigma^{\mathrm{VDM}}}}.\end{aligned} \tag{4.10}$$

The above equation explicitly demonstrates the effect of the $s\bar{s}$ admixture and the OPE process in the asymmetry. With the strangeness probability $B^2=1\%$, the $s\bar{s}$-knockout contribution to the total unpolarized cross section is only at the level of 5%. But in the asymmetry C_{zz}^{BT}, its contribution may be seen at the level of 0.45 since it is proportional to the square root of the hidden strangeness contribution to the cross section. This should be compared with the prediction of VDM plus OPE, which gives $C_{zz}^{\mathrm{BT}}\approx 0$ when the VDM amplitude is purely imaginary. The OPE contribution to the unpolarized cross section has the same order of magnitude as that of the $s\bar{s}$ knockout, and its contribution to C_{zz}^{BT} comes

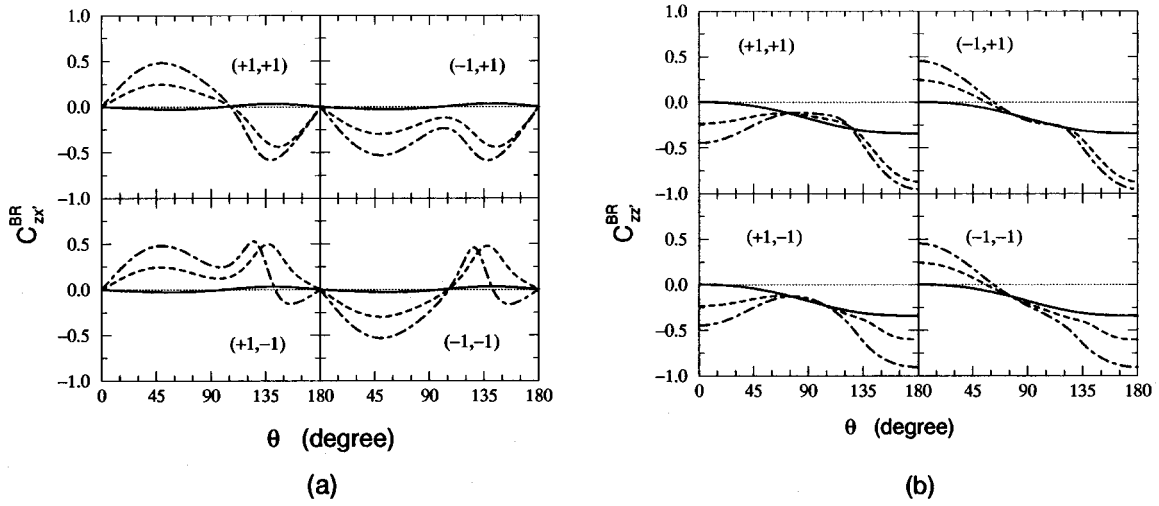

FIG. 11. Notation same as in Fig. 10 but for (a) $C_{zx'}^{\mathrm{BR}}$ and (b) $C_{zz'}^{\mathrm{BR}}$.

only from the interference with the real part of the VDM amplitude. However, this contribution is suppressed by the additional factor $\xi \sim 0.1$ and, as a result, it is at the level of 0.05 which is much smaller than the effect of hidden strangeness in the proton. Thus, in the results presented below we do not take into account the real part of the VDM amplitude.

C. Numerical results

Our results for the beam-target double asymmetry,[7] C_{ij}^{BT}, are shown in Fig. 10. Here the solid line corresponds to the VDM plus OPE prediction, and the dashed and the dot-dashed lines are the predictions when we include the knockout contributions with $B^2=0.25\%$ and 1%, respectively. Since we have no *a priori* information about the phases $\eta_{0,1}$, we give results for all four different choices of relative phases. Our numerical calculation confirms the previous qualitative considerations. One can see that C_{zz}^{BT} in Fig. 10(a) depends strongly on the hidden strangeness content of the proton *even in the forward scattering region*. This difference is caused by the different spin structures of the VDM and the knockout amplitudes. Therefore, this observable can be used to extract the hidden strangeness of the proton even for $B^2 \leqslant 1\%$. The results for C_{zx}^{BT} in Fig. 10(b) lead to the same conclusion although it is not as sensitive as in C_{zz}^{BT}. Note that the results at small θ are nearly independent of η_1. This is because the uud-knockout process is suppressed compared with other mechanisms in this region. Similarly, the results are nearly independent of the phase η_0 at large θ. From the energy dependence of the polarization observables, we observe that the knockout contribution is suppressed at higher energies because of the strong suppression due to the form factors in the knockout amplitudes. This leads to the conclusion that the optimal range of the initial photon energy needed to measure the $s\bar{s}$ component of the proton would be around 2–3 GeV. Furthermore, we find that the forward scattering region of $\theta \leqslant 30°$ offers a better opportunity to measure the hidden strangeness contribution. This conclusion holds for the other spin observables as will be seen below.

In Fig. 11, we give our results for the beam-recoil asymmetries, $C_{zx'}^{\mathrm{BR}}$ and $C_{zz'}^{\mathrm{BR}}$. This shows that these observables can be useful in probing the strangeness of the nucleon.

The target-recoil double asymmetries $C_{xz'}^{\mathrm{TR}}$ and $C_{zz'}^{\mathrm{TR}}$ are shown in Fig. 12. In this case, however, the knockout mechanism gives a very similar behavior of VDM except at large angles. Thus the observables $C_{xz'}^{\mathrm{TR}}$ and $C_{zz'}^{\mathrm{TR}}$ are *not* so useful for the purpose of extracting the knockout process. The same conclusion applies to the beam–vector-meson asymmetries C_{ij}^{BV}. As an example, we give our results in Fig. 13, which shows that $C_{zx'}^{\mathrm{BV}}$ and $C_{zz'}^{\mathrm{BV}}$ are nearly independent of the hidden strangeness content of the proton.[8]

Figure 14 shows our results for C^{TV}. We also present the predictions for C^{RV} in Fig. 15. We see that all of them show strong sensitivity to the strangeness content of the proton.

V. OTHER CONFIGURATIONS OF NUCLEON WAVE FUNCTION

In the last section, we assumed that both the $s\bar{s}$ and uud clusters are in their lowest orbital configuration, namely, S state. We label this configuration as ''configuration (I).'' In this section, we discuss the role of the orbitally excited cluster configurations in the five-quark cluster model for the nucleon in ϕ photoproduction. We consider the orbital excitation of the $s\bar{s}$ cluster, called ''configuration (II)'' and the orbitally excited uud cluster, called ''configuration (III).'' In these cases, the $s\bar{s}$ and uud clusters form a positive parity physical proton with $\ell=0$. Then we can generalize the proton wave function as

$$|p\rangle = A|[uud]^{1/2}\rangle + \sum_{\substack{n=\mathrm{I,II,III} \\ j_{s\bar{s}}=0,1}} b_{j_{s\bar{s}}}^{(n)} |[[uud]^{j_n} \otimes [s\bar{s}]^{j_{s\bar{s}}} \otimes [\mathbf{L}]]^{1/2}\rangle, \tag{5.1}$$

where the superscripts j_n and $j_{s\bar{s}}$ denote the spin of each cluster and $|b_0^{(n)}|^2$ and $|b_1^{(n)}|^2$ correspond to the spin-0 and

[7]Note that our C_{zz}^{BT} corresponds to the minus of $\mathcal{L}_{\mathrm{BT}}$ of Ref. [33].

[8]Note that the quantities C_{ij}^{BV}, C_{ij}^{TV}, and C_{ij}^{RV} with $(j = x', y', z')$ are defined to vary between $\pm\sqrt{3/2}$ [38].

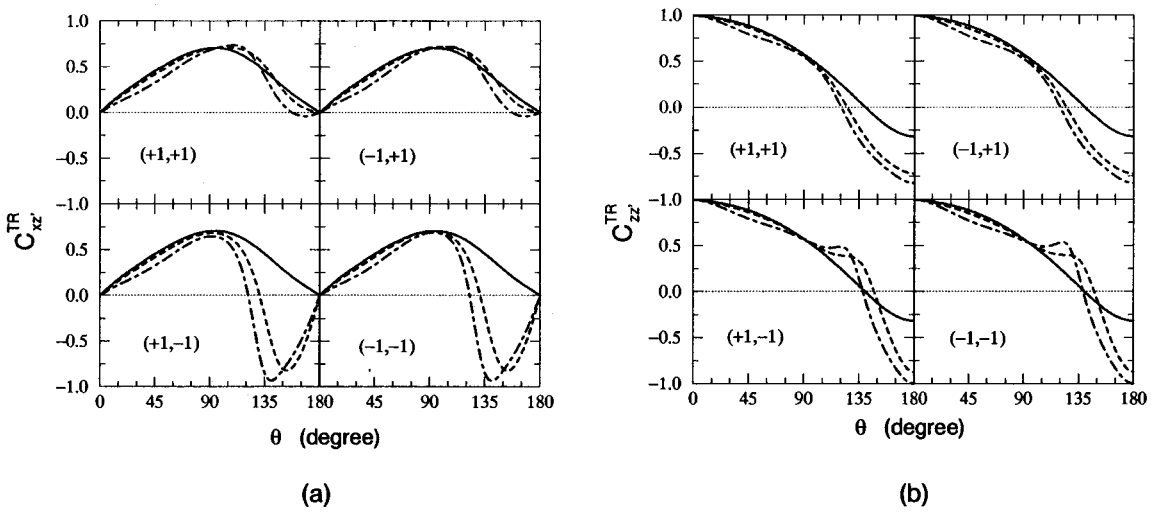

FIG. 12. Notation same as in Fig. 10 but for (a) $C^{TR}_{xz'}$ and (b) $C^{TR}_{zz'}$.

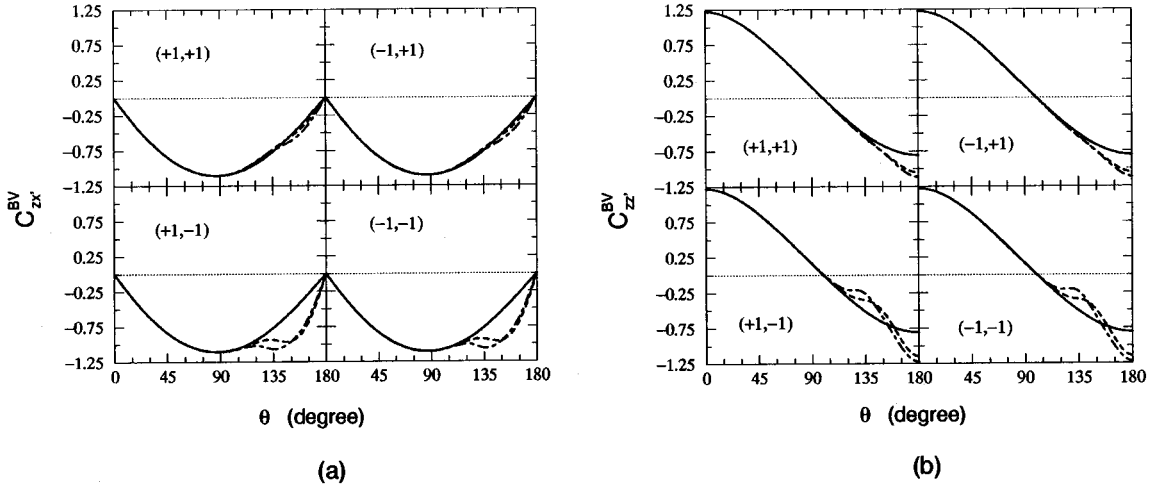

FIG. 13. Notation same as in Fig. 10 but for (a) $C^{BV}_{zx'}$ and (b) $C^{BV}_{zz'}$.

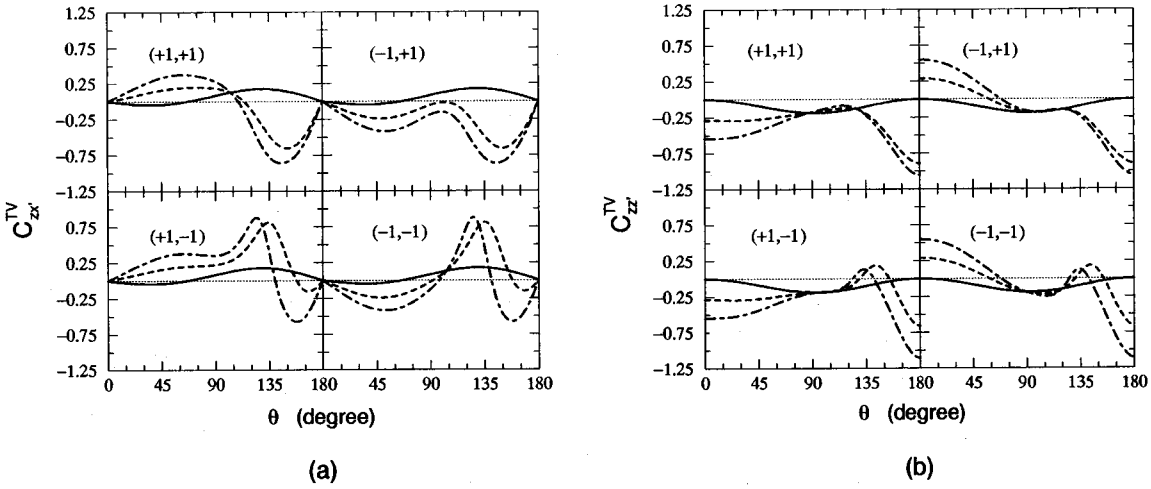

FIG. 14. Notation same as in Fig. 10 but for (a) $C^{TV}_{zx'}$ and (b) $C^{TV}_{zz'}$.

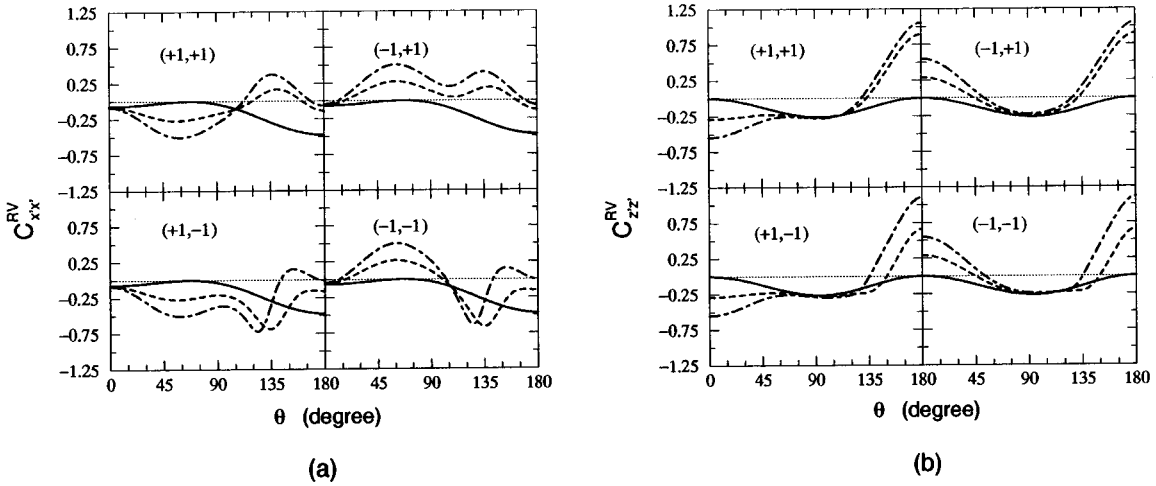

FIG. 15. Notation same as in Fig. 10 but for (a) $C^{\mathrm{RV}}_{x'x'}$ and (b) $C^{\mathrm{RV}}_{z'z'}$.

spin-1 amplitudes of the $s\bar{s}$ cluster of ''configuration (n),'' respectively. B^2, the strangeness admixture of the proton, is then $\Sigma(b^{(n)}_{j_{s\bar{s}}})^2$. The amplitudes are constrained to be $A^2+B^2=A^2+\Sigma(b^{(n)}_{j_{s\bar{s}}})^2=1$ by the normalization of the wave function.

The symmetry properties of the wave functions in the initial and final states lead to the selection rules for different $s\bar{s}$ configurations as summarized in Table I. We find that from six possible terms of the proton wave function (5.1), only four can contribute to the direct knockout process: two in $s\bar{s}$ knockout and two in uud knockout. The other two amplitudes do not contribute to the direct knockout process, although they can give a contribution to the total hidden strangeness probability.

By analyzing the amplitudes one can find that the electric transition is suppressed by the magnetic as in the case of configuration (I) [30]. For example, the suppression factor for configuration (II) reads

$$f_{(\mathrm{II})}=\frac{|\mathbf{p}'_L|\sin\theta_{p'}}{E^L_\gamma}, \tag{5.2}$$

which can be expressed in the invariant form as

$$f^2_{(\mathrm{II})}=-2M_N^2\frac{W^2t^2+[W^2(W^2-2M_N^2-M_\phi^2)+M_N^2(M_N^2-M_\phi^2)t]+M_\phi^4M_N^2}{(W^2-M_N^2)^4}. \tag{5.3}$$

Numerical estimation shows that with $W\sim 2.1$ GeV the suppression factor $f^2_{(\mathrm{II})}$ reaches its maximum value around 0.02 at $t\sim -0.8$ GeV^2 and it becomes negligibly small as $|t|\to|t|_{\max}$ or $|t|\to|t|_{\min}$. A similar suppression factor appears in the electric transition of uud knockout in configuration (III). Thus in the region of t of interest to us, where the knockout mechanism would be important, the contribution of the electric transitions is negligible and we will consider the magnetic transitions only.

The amplitudes for configurations (II) and (III) can be calculated in a straightforward way using the method of Refs. [29,30]. The corresponding amplitudes have the form as given in Eq. (3.32) by replacing T_0 and $\mathcal{S}$ by

$$T_0^{s\bar{s}(\mathrm{II})}=\left(\frac{8\pi\alpha_e E^L_\phi E^L_{p'}}{M_N}\right)^{1/2}A^*b_0^{(\mathrm{II})}F^{(\mathrm{II})}_{s\bar{s}}(\gamma^L_\phi,q_{s\bar{s}})F^{(\mathrm{I})}_{uud}(\gamma^L_{p'},0)\bar{V}_{s\bar{s}}(\mathbf{p}'_L)\frac{\mu_s E^L_\gamma}{3M_N}, \tag{5.4}$$

$$\mathcal{S}^{s\bar{s}(\mathrm{II})}_{fi}=-\lambda_\gamma\sqrt{3}\sum_{j_c=0,1}\langle 1m_s10|j_cm_s\rangle\langle\tfrac{1}{2}m_fj_cm_s|\tfrac{1}{2}m_i\rangle\langle 1m_s1\lambda_i|1m_\phi\rangle, \tag{5.5}$$

for ''configuration (II)'' and

$$T_0^{uud(\mathrm{III})}=\left(\frac{8\pi\alpha_e E^L_\phi E^L_{p'}}{M_N}\right)^{1/2}A^*b_1^{(\mathrm{III})}F^{(\mathrm{I})}_{s\bar{s}}(\gamma^L_\phi,0)F^{(\mathrm{III})}_{uud}(\gamma^L_{p'},q_{uud})\bar{V}_{uud}(\mathbf{q}_L)\frac{\mu E^L_\gamma}{2M_N}, \tag{5.6}$$

$$\mathcal{S}^{uud(\mathrm{III})}_{fi}=-\sqrt{\frac{3}{2}}\sum_{j_c=1/2,3/2}\langle j_cm_f-\lambda_\gamma1m_\phi|\tfrac{1}{2}m_i\rangle\langle\tfrac{1}{2}m_f-\lambda_\gamma10|j_cm_f-\lambda_\gamma\rangle, \tag{5.7}$$

TABLE I. Selection rules of knockout processes for each quark configuration of the nucleon. The electric and magnetic transitions are represented by E and M, respectively.

Configuration	I		II		III	
$S_{s\bar{s}}$	0	1	0	1	0	1
$s\bar{s}$ knockout	M	—	—	E, M	—	—
uud knockout	—	E, M	—	—	—	E, M

for ''configuration (III).'' The functions $F_\beta^{(\mathrm{II}),(\mathrm{III})}$ with $\beta=(s\bar{s},uud)$ are related to the correspondent $F_\beta^{(\mathrm{I})}$ of Eq. (3.36) as

$$F_{s\bar{s}}^{(\mathrm{II})}(\gamma_\phi^L,q_{s\bar{s}})=\frac{E_\gamma^L\sqrt{r_{s\bar{s}}^2}(1-V_{q\|})}{3}F_{s\bar{s}}^{(\mathrm{I})}(\gamma_\phi^L,q_{s\bar{s}}),$$

$$F_{uud}^{(\mathrm{III})}(\gamma_{p'}^L,q_{uud})=\frac{E_\gamma^L\sqrt{r_{uud}^2}(1-V_{p'\|})}{3}F_{uud}^{(\mathrm{I})}(\gamma_{p'}^L,q_{uud}), \tag{5.8}$$

where $V_{p\|}=|\mathbf{p}|\cos\theta_p/E_p^L$. The momentum distribution function $\bar{v}_\beta(p)$ of cluster β is given by

$$\frac{1}{(2\pi)^3}\bar{V}_\beta(\mathbf{p})=\frac{\bar{v}_\beta(\mathbf{p})}{\int d\mathbf{p}v_\beta^{(0)}(\mathbf{p})},$$

$$\bar{v}_\beta(\mathbf{p})=\exp\left\{-\frac{5}{3\Omega_\chi}(\mathbf{p}^2-x_\beta M_N E_\beta)\right\}. \tag{5.9}$$

Note that the difference with v_β of Eq. (3.38) lies in the absence of the factor $\mathbf{p}^2$. The calculation of $T^{s\bar{s}(\mathrm{II})}$ is rather similar to that of $T^{s\bar{s}(\mathrm{I})}$ which is given in Ref. [30] and Appendix E contains the derivation of $T^{s\bar{s}(\mathrm{III})}$ in some detail.

Analyses of the relative contribution from different cluster configurations show that the contribution of configurations (II) and (III) are much smaller (by an order of magnitude) than that of configuration (I) even if we assume the same values for $b_{0,1}^{(n)}$. This can be seen from Fig. 16 where we present our results for the differential cross sections from each configuration.

For clarity, let us consider the $s\bar{s}$ knockout for configurations (I) and (II). The ratio of the spatial matrix elements for configurations (I) and (II) read

$$R_{s\bar{s}}=\frac{E_\gamma^L(1-V_{q\|})\sqrt{r_{s\bar{s}}^2}}{|\mathbf{p}_L'|}\frac{N_{\mathrm{II}}}{3N_{\mathrm{I}}}, \tag{5.10}$$

where $N_{\mathrm{I,II}}$ are the normalization factors of the radial wave functions of configurations (I) and (II), respectively. Since

$$N_\alpha^{-2}\sim\int d\mathbf{p}v_\alpha(\mathbf{p}), \tag{5.11}$$

we can obtain

$$\frac{N_{\mathrm{II}}}{N_{\mathrm{I}}}\simeq\sqrt{\frac{3\Omega_\chi}{2}}. \tag{5.12}$$

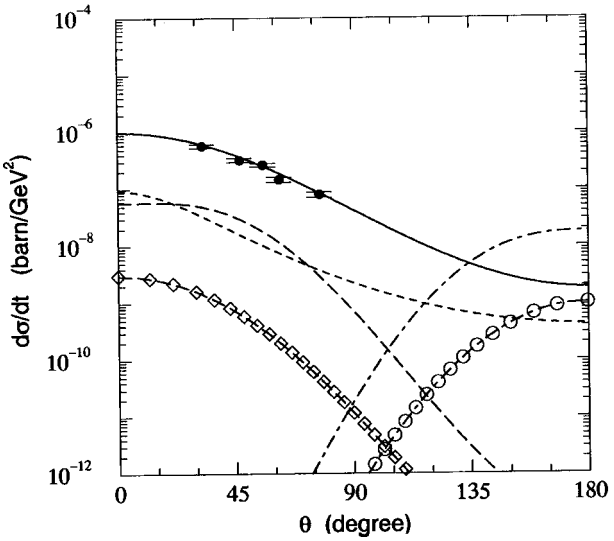

FIG. 16. The unpolarized photoproduction cross section $d\sigma/dt(\theta)$ at $W=2.155$ GeV ($E_\gamma^L=2.0$ GeV). The solid and dotted lines give the cross section of VDM and OPE. The dashed and dot-dashed lines are from the $s\bar{s}$ and uud knockout from configuration (I) in the proton wave function. The dashed line with diamonds and the dot-dashed line with circles are the cross sections from the $s\bar{s}$ and uud knockout by assuming only configurations (II) and (III) in the nucleon, respectively. The strangeness admixture is assumed to be $B^2=1\%$ and $|b_0^{(n)}|=|b_1^{(n)}|=B/\sqrt{2}$. The experimental data are from Ref. [59].

Using the numerical value of the dimensional parameters $r_{s\bar{s}}=0.29$ fm and $\sqrt{\Omega_\chi}=2.63$ fm^{-1} [30], we obtain

$$R_{s\bar{s}}\simeq 0.31\frac{E_\gamma^L(1-V_{q\|})}{|\mathbf{p}_L'|}. \tag{5.13}$$

Since at $\theta\simeq 0$ we have $\cos\theta_{p'}\simeq\cos\theta_\phi\simeq 1$, $E_\phi^L=E_\gamma^L+t/2M_N\simeq E_\gamma^L$, and

$$|\mathbf{p}_L'|=|\mathbf{k}_L|-|\mathbf{q}_L|\simeq E_\gamma^L\left(1-\frac{|\mathbf{q}_L|}{E_\phi^L}\right)=E_\gamma^L(1-V_{q\|}), \tag{5.14}$$

we then obtain $R_{s\bar{s}}^2\simeq 0.1$, which agrees with the numerical calculation of Fig. 16. A similar conclusion can be drawn for the uud knockout from configurations (I) and (III).

The above analysis shows that the cross section of the knockout process is dominated by configuration (I) and we can safely neglect the other cluster configurations in the proton wave function. Now let us consider the polarization observables. For simplicity, we again consider the case of configuration (II). From the amplitude (5.5), one can find

$$H_{\lambda_f,\lambda_\phi;\lambda_\gamma,\lambda_i}^{s\bar{s}(\mathrm{II})}\propto\delta_{\lambda_f\lambda_i}\delta_{\lambda_\phi\lambda_\gamma}. \tag{5.15}$$

This has the same structure as the VDM helicity amplitude (4.2). Since its amplitude is suppressed by the dominant VDM amplitude, however, it cannot be extracted from the background VDM contribution. We could verify this analysis by numerical calculation even with the assumption of the same values for $b_{j_{s\bar{s}}}^{(n)}$. Furthermore, because of their heavy

mass, the coefficients $b_{0,1}$ of configurations (II) and (III) are expected to be much smaller than those of configuration (I). As a conclusion, therefore, the contributions from the orbitally excited cluster configurations can be neglected in the polarization observables as well.

VI. SUMMARY AND CONCLUSION

We have studied the possibility of using the spin observables of the ϕ meson photoproduction process in probing the hidden strangeness content of the proton. We consider the direct knockout mechanism in addition to the VDM and OPE processes by assuming an $s\bar{s}$ component in the proton wave function. Unlike the differential cross section, we find that the spin observables could be useful in disentangling the knockout process from the VDM and OPE processes. We find that single polarization observables are *not* sensitive to the strangeness content of the proton. However, some double polarization observables, notably, $C^{\rm BT}_{zx,zz}$, $C^{\rm BR}_{zx',zz'}$, $C^{\rm TV}_{zx',zz'}$, and $C^{\rm RV}_{x'x',z'z'}$, are *very sensitive* to the hidden strangeness content of the proton in the forward scattering region, whereas most of the target-recoil and beam–vector-meson double asymmetries are not. It indicates that measurements of these double polarization observables could be very useful in probing the strangeness content of the proton.

We also find that the contribution of the knockout mechanism is suppressed with increasing initial photon energy because of the strong suppression due to the form factors in the knockout amplitudes. Therefore, we expect that the optimal range of the initial photon energy needed to measure the $s\bar{s}$ component of the proton would be around 2–3 GeV. However, it should be mentioned that at extremely low energy just near the threshold one has to take into account the OZI evading rescattering process and it would be interesting to study its effect on the polarization observables.

The orbitally excited quark cluster configurations in the proton wave function were also investigated in connection with ϕ photoproduction. We find that their role is *not* important in the cross section and polarization observables and, therefore, these configurations can be neglected in the study of ϕ photoproduction.

The purpose of this study is to determine the strangeness content of the proton by investigating the polarization observables. Unfortunately, because of the scarcity of presently available experimental data [64,65], we cannot give any definite predictions for the strangeness content of the proton based on our analyses. Thus, new experiments are strongly called for at the current electron facilities which, hopefully, will help to shed light on our understanding of the proton structure.

Finally, we point out that, since the $s\bar{s}$-knockout process dominates the uud knockout at the forward scattering angle, one can estimate the value of b_0 in the proton wave function (3.30) by analyzing polarization observables. However, it is not easy to get an estimate for b_1 because its contribution can be seen only at large θ where corrections to our model are expected to be important. To get information for b_1, therefore, it would be interesting to apply our analyses to $\eta(\eta')$ photoproduction as a complementary process to ϕ photoproduction, since the $s\bar{s}$-knockout process in this case is associated with b_1.

ACKNOWLEDGMENTS

We gratefully acknowledge useful discussions with M. Fujiwara, S. B. Gerasimov, S. V. Goloskokov, C. R. Ji, T. Kinashi, and M. Namiki. Y.O. is also grateful to D.-P. Min for encouragement and wishes to thank the Physics Department and the Center for Theoretical Sciences of the National Taiwan University for the warm hospitality. A.I.T. appreciates the warm hospitality of the Faculty of Human Development of Kobe University where part of this work was carried out. This work was supported in part by the Russian Foundation for Basic Research under Grant No. 96-15-96423, the Korea Science and Engineering Foundation through the Center for Theoretical Physics of Seoul National University, the National Science Council of ROC under Grant No. NSC87-2112-M-002, and Monbusho's Special Program for Promoting Advanced Study (1996, Japan). Lastly we thank A. Jackson of Kobe Shoin Women's College for careful reading of the manuscript.

APPENDIX A: DENSITY MATRICES

In this appendix, we discuss the density matrices of the photon, target and recoil proton, and the vector meson. In general, the density matrix of the photon can be written as

$$\rho_\gamma=\frac{1}{2}(\mathbf{1}_2+\boldsymbol{\sigma}_\gamma\cdot\mathbf{P}_S), \tag{A1}$$

in photon helicity space, where $\mathbf{1}_2$ is the 2×2 unit matrix and $\mathbf{P}_S$ is the Stokes vector which defines the direction and degree of polarization of the photon beam. The presence of $\boldsymbol{\sigma}_\gamma$ is due to the fact that a real photon has only two spin degrees of freedom. The Stokes vectors corresponding to some special cases of photon polarization can be found, for example, in Ref. [44].

The proton density matrix is in the spin-$\frac{1}{2}$ space and is therefore a 2×2 Hermitian matrix. So we have

$$\rho_N=\frac{1}{2}(\mathbf{1}_2+\boldsymbol{\sigma}_N\cdot\mathbf{P}_N), \tag{A2}$$

for the target proton and

$$\rho_{N'}=\frac{1}{2}(\mathbf{1}_2+\boldsymbol{\sigma}_{N'}\cdot\mathbf{P}_{N'}), \tag{A3}$$

for the recoil proton.

For the vector meson, because of its spin-1 structure, the density matrix cannot be described by vector polarizations only. To describe the vector meson polarization completely, we have to take into account the tensor polarizations. The tensor polarization operator is defined as [39,40]

$$S_{jk}=\frac{3}{2}(S_jS_k+S_kS_j)-2\,\delta_{jk}\mathbf{1}_3, \tag{A4}$$

where $\mathbf{1}_3$ is the 3×3 unit matrix with

$$S_x=\frac{1}{\sqrt{2}}\begin{pmatrix}0&1&0\\1&0&1\\0&1&0\end{pmatrix},\quad S_y=\frac{1}{\sqrt{2}}\begin{pmatrix}0&-i&0\\i&0&-i\\0&i&0\end{pmatrix},$$

$$S_z=\begin{pmatrix}1&0&0\\0&0&0\\0&0&-1\end{pmatrix}. \tag{A5}$$

Only five of them are independent since $S_{xx}+S_{yy}+S_{zz}=0$. Therefore, we are led to the final form of the density matrix of vector meson as

$$\rho_V=\frac{1}{3}\left(\mathbf{1}_3+\sum_j P_j^V\Omega_j^V\right), \tag{A6}$$

where

$$\Omega_j^V=\sqrt{\frac{3}{2}}(S_x,S_y,S_z),\quad \frac{1}{\sqrt{6}}(S_{xx}-S_{yy}),$$
$$\frac{1}{\sqrt{2}}S_{zz},\quad \sqrt{\frac{2}{3}}(S_{xy},S_{yz},S_{zx}), \tag{A7}$$

which are normalized as $\mathrm{Tr}\,\Omega_j^V\Omega_k^V=3\delta_{jk}$.

The explicit forms of the matrices appearing in Eq. (2.11) are $(\mathbf{1}_2,\boldsymbol{\sigma}_\gamma)$ for A_γ, $(\mathbf{1}_2,\boldsymbol{\sigma}_{N(N')})$ for A_N $(B_{N'})$, and $(\mathbf{1}_3,\Omega_j^V)$ for B_V.[9]

APPENDIX B: SINGLE AND DOUBLE POLARIZATION OBSERVABLES IN HELICITY AMPLITUDES

In this appendix, we give the explicit expressions for the spin observables in terms of helicity amplitudes.

The cross section intensity $\mathcal{I}(\theta)$ is defined as

$$\mathcal{I}(\theta)=\frac{1}{4}\mathrm{Tr}\,(\mathcal{F}\mathcal{F}^\dagger), \tag{B1}$$

which leads to

$$\mathcal{I}(\theta)=\frac{1}{2}\sum_{i=1}^{4}\sum_{a=\pm1,0}|H_{i,a}|^2. \tag{B2}$$

The explicit expressions for nonvanishing single polarization observables are as follows:

$$\Sigma_x\cdot\mathcal{I}(\theta)=-\mathrm{Re}\{H_{4,1}^*H_{1,-1}-H_{4,0}^*H_{1,0}+H_{4,-1}^*H_{1,1}-H_{3,1}^*H_{2,-1}+H_{3,0}^*H_{2,0}-H_{3,-1}^*H_{2,1}\}, \tag{B3a}$$

$$T_y\cdot\mathcal{I}(\theta)=-\mathrm{Im}\,\{H_{4,-1}^*H_{3,-1}+H_{4,0}^*H_{3,0}+H_{4,1}^*H_{3,1}+H_{2,-1}^*H_{1,-1}+H_{2,0}^*H_{1,0}+H_{2,1}^*H_{1,1}\}, \tag{B3b}$$

$$P_{y'}\cdot\mathcal{I}(\theta)=-\mathrm{Im}\,\{H_{4,-1}^*H_{2,-1}+H_{4,0}^*H_{2,0}+H_{4,1}^*H_{2,1}+H_{3,-1}^*H_{1,-1}+H_{3,0}^*H_{1,0}+H_{3,1}^*H_{1,1}\}, \tag{B3c}$$

$$V_{y'}\cdot\mathcal{I}(\theta)=-\frac{\sqrt{3}}{2}\mathrm{Im}\,\{H_{4,0}^*(H_{4,1}-H_{4,-1})+H_{3,0}^*(H_{3,1}-H_{3,-1})+H_{2,0}^*(H_{2,1}-H_{2,-1})+H_{1,0}^*(H_{1,1}-H_{1,-1})\}, \tag{B3d}$$

$$V_{x'x'y'y'}\cdot\mathcal{I}(\theta)=\sqrt{\frac{3}{2}}\mathrm{Re}\{H_{4,-1}^*H_{4,1}+H_{3,-1}^*H_{3,1}+H_{2,-1}^*H_{2,1}+H_{1,-1}^*H_{1,1}\}, \tag{B3e}$$

$$V_{z'z'}\cdot\mathcal{I}(\theta)=\frac{1}{2\sqrt{2}}\{|H_{4,-1}|^2-2|H_{4,0}|^2+|H_{4,1}|^2+|H_{3,-1}|^2-2|H_{3,0}|^2+|H_{3,1}|^2+|H_{2,-1}|^2-2|H_{2,0}|^2+|H_{2,1}|^2+|H_{1,-1}|^2$$
$$-2|H_{1,0}|^2+|H_{1,1}|^2\}, \tag{B3f}$$

$$V_{z'x'}\cdot\mathcal{I}(\theta)=\frac{\sqrt{3}}{2}\mathrm{Re}\{H_{4,0}^*(H_{4,1}-H_{4,-1})+H_{3,0}^*(H_{3,1}-H_{3,-1})+H_{2,0}^*(H_{2,1}-H_{2,-1})+H_{1,0}^*(H_{1,1}-H_{1,-1})\}, \tag{B3g}$$

The explicit expressions for some double polarization observables are given below.

Beam-target:

$$C_{yx}^{\mathrm{BT}}\cdot\mathcal{I}(\theta)=\mathrm{Im}\,\{H_{4,-1}^*H_{2,1}-H_{4,0}^*H_{2,0}+H_{4,1}^*H_{2,-1}-H_{3,-1}^*H_{1,1}+H_{3,0}^*H_{1,0}-H_{3,1}^*H_{1,-1}\}, \tag{B4a}$$

$$C_{yz}^{\mathrm{BT}}\cdot\mathcal{I}(\theta)=-\mathrm{Im}\,\{H_{4,-1}^*H_{1,1}-H_{4,0}^*H_{1,0}+H_{4,1}^*H_{1,-1}+H_{3,-1}^*H_{2,1}-H_{3,0}^*H_{2,0}+H_{3,1}^*H_{2,-1}\}, \tag{B4b}$$

$$C_{zx}^{\mathrm{BT}}\cdot\mathcal{I}(\theta)=-\mathrm{Re}\,\{H_{4,-1}^*H_{3,-1}+H_{4,0}^*H_{3,0}+H_{4,1}^*H_{3,1}+H_{2,-1}^*H_{1,-1}+H_{2,0}^*H_{1,0}+H_{2,1}^*H_{1,1}\}, \tag{B4c}$$

[9]One has to use $-\sigma_x$ and $-\sigma_z$ for the initial and final protons instead of σ_x and σ_z in order to have the correct helicity states in the c.m. system [44].

$$C_{zz}^{\mathrm{BT}}\cdot\mathcal{I}(\theta)=-\frac{1}{2}\{|H_{4,-1}|^2+|H_{4,0}|^2+|H_{4,1}|^2-|H_{3,-1}|^2-|H_{3,0}|^2-|H_{3,1}|^2+|H_{2,-1}|^2+|H_{2,0}|^2 + |H_{2,1}|^2-|H_{1,-1}|^2-|H_{1,0}|^2-|H_{1,1}|^2\}. \tag{B4d}$$

Beam-recoil:

$$C_{yx'}^{\mathrm{BR}}\cdot\mathcal{I}(\theta)=\mathrm{Im}\{H_{4,-1}^*H_{3,1}-H_{4,0}^*H_{3,0}+H_{4,1}^*H_{3,-1}-H_{2,-1}^*H_{1,1}+H_{2,0}^*H_{1,0}-H_{2,1}^*H_{1,-1}\}, \tag{B5a}$$

$$C_{yz'}^{\mathrm{BR}}\cdot\mathcal{I}(\theta)=\mathrm{Im}\{H_{4,-1}^*H_{1,1}-H_{4,0}^*H_{1,0}+H_{4,1}^*H_{1,-1}-H_{3,-1}^*H_{2,1}+H_{3,0}^*H_{2,0}-H_{3,1}^*H_{2,-1}\}, \tag{B5b}$$

$$C_{zx'}^{\mathrm{BR}}\cdot\mathcal{I}(\theta)=-\mathrm{Re}\{H_{4,-1}^*H_{2,-1}+H_{4,0}^*H_{2,0}+H_{4,1}^*H_{2,1}+H_{3,-1}^*H_{1,-1}+H_{3,0}^*H_{1,0}+H_{3,1}^*H_{1,1}\}, \tag{B5c}$$

$$C_{zz'}^{\mathrm{BR}}\cdot\mathcal{I}(\theta)=\frac{1}{2}\{|H_{4,-1}|^2+|H_{4,0}|^2+|H_{4,1}|^2+|H_{3,-1}|^2+|H_{3,0}|^2+|H_{3,1}|^2-|H_{2,-1}|^2-|H_{2,0}|^2 - |H_{2,1}|^2-|H_{1,-1}|^2-|H_{1,0}|^2-|H_{1,1}|^2\}. \tag{B5d}$$

Target-recoil:

$$C_{xx'}^{\mathrm{TR}}\cdot\mathcal{I}(\theta)=\mathrm{Re}\{H_{4,-1}^*H_{1,-1}+H_{4,0}^*H_{1,0}+H_{4,1}^*H_{1,1}+H_{3,-1}^*H_{2,-1}+H_{3,0}^*H_{2,0}+H_{3,1}^*H_{2,1}\}, \tag{B6a}$$

$$C_{xz'}^{\mathrm{TR}}\cdot\mathcal{I}(\theta)=-\mathrm{Re}\{H_{4,-1}^*H_{3,-1}+H_{4,0}^*H_{3,0}+H_{4,1}^*H_{3,1}-H_{2,-1}^*H_{1,-1}-H_{2,0}^*H_{1,0}-H_{2,1}^*H_{1,1}\}, \tag{B6b}$$

$$C_{zx'}^{\mathrm{TR}}\cdot\mathcal{I}(\theta)=\mathrm{Re}\{H_{4,-1}^*H_{2,-1}+H_{4,0}^*H_{2,0}+H_{4,1}^*H_{2,1}-H_{3,-1}^*H_{1,-1}-H_{3,0}^*H_{1,0}-H_{3,1}^*H_{1,1}\}, \tag{B6c}$$

$$C_{zz'}^{\mathrm{TR}}\cdot\mathcal{I}(\theta)=-\frac{1}{2}\{|H_{4,-1}|^2+|H_{4,0}|^2+|H_{4,1}|^2-|H_{3,-1}|^2-|H_{3,0}|^2-|H_{3,1}|^2-|H_{2,-1}|^2-|H_{2,0}|^2 - |H_{2,1}|^2+|H_{1,-1}|^2+|H_{1,0}|^2+|H_{1,1}|^2\}. \tag{B6d}$$

Beam–vector-meson:

$$C_{yx'}^{\mathrm{BV}}\cdot\mathcal{I}(\theta)=-\frac{\sqrt{3}}{2}\mathrm{Im}\{H_{4,-1}^*H_{1,0}-H_{4,0}^*(H_{1,-1}+H_{1,1})+H_{4,1}^*H_{1,0}-H_{3,-1}^*H_{2,0}+H_{3,0}^*(H_{2,-1}+H_{2,1})-H_{3,1}^*H_{2,0}\}, \tag{B7a}$$

$$C_{yz'}^{\mathrm{BV}}\cdot\mathcal{I}(\theta)=-\sqrt{\frac{3}{2}}\mathrm{Im}\{H_{4,-1}^*H_{1,1}-H_{4,1}^*H_{1,-1}-H_{3,-1}^*H_{2,1}+H_{3,1}^*H_{2,-1}\}, \tag{B7b}$$

$$C_{zx'}^{\mathrm{BV}}\cdot\mathcal{I}(\theta)=\frac{\sqrt{3}}{2}\mathrm{Re}\{H_{4,0}^*(H_{4,-1}+H_{4,1})+H_{3,0}^*(H_{3,-1}+H_{3,1})+H_{2,0}^*(H_{2,-1}+H_{2,1})+H_{1,0}^*(H_{1,-1}+H_{1,1})\}, \tag{B7c}$$

$$C_{zz'}^{\mathrm{BV}}\cdot\mathcal{I}(\theta)=-\frac{1}{2}\sqrt{\frac{3}{2}}\{|H_{4,-1}|^2-|H_{4,1}|^2+|H_{3,-1}|^2-|H_{3,1}|^2+|H_{2,-1}|^2-|H_{2,1}|^2+|H_{1,-1}|^2-|H_{1,1}|^2\}. \tag{B7d}$$

Target–vector-meson:

$$C_{xx'}^{\mathrm{TV}}\cdot\mathcal{I}(\theta)=-\frac{\sqrt{3}}{2}\mathrm{Re}\{H_{4,0}^*(H_{3,-1}+H_{3,1})+H_{3,0}^*(H_{4,-1}+H_{4,1})+H_{2,0}^*(H_{1,-1}+H_{1,1})+H_{1,0}^*(H_{2,-1}+H_{2,1})\}, \tag{B8a}$$

$$C_{xz'}^{\mathrm{TV}}\cdot\mathcal{I}(\theta)=\sqrt{\frac{3}{2}}\mathrm{Re}\{H_{4,-1}^*H_{3,-1}-H_{4,1}^*H_{3,1}+H_{2,-1}^*H_{1,-1}-H_{2,1}^*H_{1,1}\}, \tag{B8b}$$

$$C_{zx'}^{\mathrm{TV}}\cdot\mathcal{I}(\theta)=-\frac{\sqrt{3}}{2}\mathrm{Re}\{H_{4,0}^*(H_{4,-1}+H_{4,1})-H_{3,0}^*(H_{3,-1}+H_{3,1})+H_{2,0}^*(H_{2,-1}+H_{2,1})-H_{1,0}^*(H_{1,-1}+H_{1,1})\}, \tag{B8c}$$

$$C_{zz'}^{\mathrm{TV}}\cdot\mathcal{I}(\theta)=\frac{1}{2}\sqrt{\frac{3}{2}}\{|H_{4,-1}|^2-|H_{4,1}|^2-|H_{3,-1}|^2+|H_{3,1}|^2+|H_{2,-1}|^2-|H_{2,1}|^2-|H_{1,-1}|^2+|H_{1,1}|^2\}. \tag{B8d}$$

Recoil−vector-meson:

$$C^{\mathrm{RV}}_{x'x'}\cdot\mathcal{I}(\theta)=-\frac{\sqrt{3}}{2}\mathrm{Re}\{H^*_{4,0}(H_{2,-1}+H_{2,1})+H^*_{3,0}(H_{1,-1}+H_{1,1})+H^*_{2,0}(H_{4,-1}+H_{4,1})+H^*_{1,0}(H_{3,-1}+H_{3,1})\},\tag{B9a}$$

$$C^{\mathrm{RV}}_{x'z'}\cdot\mathcal{I}(\theta)=\sqrt{\frac{3}{2}}\mathrm{Re}\{H^*_{4,-1}H_{2,-1}-H^*_{4,1}H_{2,1}+H^*_{3,-1}H_{1,-1}-H^*_{3,1}H_{1,1}\},\tag{B9b}$$

$$C^{\mathrm{RV}}_{z'x'}\cdot\mathcal{I}(\theta)=\frac{\sqrt{3}}{2}\mathrm{Re}\{H^*_{4,0}(H_{4,-1}+H_{4,1})+H^*_{3,0}(H_{3,-1}+H_{3,1})-H^*_{2,0}(H_{2,-1}+H_{2,1})-H^*_{1,0}(H_{1,-1}+H_{1,1})\},\tag{B9c}$$

$$C^{\mathrm{RV}}_{z'z'}\cdot\mathcal{I}(\theta)=-\frac{1}{2}\sqrt{\frac{3}{2}}\{|H_{4,-1}|^2-|H_{4,1}|^2+|H_{3,-1}|^2-|H_{3,1}|^2-|H_{2,-1}|^2+|H_{2,1}|^2-|H_{1,-1}|^2+|H_{1,1}|^2\}.\tag{B9d}$$

APPENDIX C: MODELS ON THE VDM AMPLITUDE

In Sec. III A, we write the invariant amplitude of the diffractive production as

$$T^{\mathrm{VDM}}_{fi}=iT_0\varepsilon^*_{\phi\mu}\mathcal{M}^{\mu\nu}\varepsilon_{\gamma\nu},\tag{C1}$$

with $\mathcal{M}^{\mu\nu}=\mathcal{F}_\alpha\Gamma^{\alpha,\mu\nu}$, where $\mathcal{F}_\alpha$ and $\Gamma^{\alpha,\mu\nu}$ correspond to the Pomeron-nucleon vertex and Pomeron−photon−vector-meson vertex, respectively. In Ref. [33], we used

$$\tilde{\Gamma}^{\alpha,\mu\nu}=(k+q)^\alpha g^{\mu\nu}-k^\mu g^{\alpha\nu}-q^\nu g^{\alpha\mu},\tag{C2}$$

instead of the $\Gamma^{\alpha,\mu\nu}$ of Eq. (3.8). This expression comes from gauging the massive-vector field Lagrangian for the $\phi\phi\mathbb{P}$ interaction which is assumed to have the same spin structure as the $\phi\phi\gamma$ vertex. However, it does not satisfy the gauge invariance condition $q_\mu\mathcal{M}^{\mu\nu}=\mathcal{M}^{\mu\nu}k_\nu=0$. One way to get a gauge invariant amplitude is to multiply $\tilde{\Gamma}^{\alpha,\mu\nu}$ by the projection operator $\mathcal{P}_{\mu\nu}$ as in Sec. III,

$$\begin{aligned}\tilde{\Gamma}^{\alpha,\mu\nu}\to\tilde{\Gamma}^{\alpha,\mu\nu}_1&=\mathcal{P}^{\mu\mu'}\tilde{\Gamma}^\alpha_{\mu'\nu'}\mathcal{P}^{\nu'\nu}\\&=(k+q)^\alpha g^{\mu\nu}-\frac{(k+q)^\alpha}{k\cdot q}k^\mu q^\nu.\end{aligned}\tag{C3}$$

Another way to project the gauge noninvariant part out of $\tilde{\Gamma}^{\alpha,\mu\nu}$ is to multiply $\mathcal{P}^{\mu\nu}_{(l)}$ and $\mathcal{P}^{\mu\nu}_{(r)}$ as

$$\tilde{\Gamma}^{\alpha,\mu\nu}\to\tilde{\Gamma}^{\alpha,\mu\nu}_2=\mathcal{P}^{\mu\mu'}_{(l)}\tilde{\Gamma}^\alpha_{\mu'\nu'}\mathcal{P}^{\nu'\nu}_{(r)},\tag{C4}$$

where

$$\mathcal{P}^{\mu\nu}_{(l)}=g^{\mu\nu}-\frac{1}{q^2}q^\mu q^\nu,$$

$$\mathcal{P}^{\mu\nu}_{(r)}=g^{\mu\nu}-\frac{1}{k^2}k^\mu k^\nu.\tag{C5}$$

This gives us

$$\begin{aligned}\tilde{\Gamma}^{\alpha,\mu\nu}_2=&(k+q)^\alpha g^{\mu\nu}-k^\mu g^{\alpha\nu}-q^\nu g^{\alpha\mu}\\&-\frac{1}{q^2}q^\mu(k^\alpha q^\nu-k\cdot qg^{\alpha\nu})-\frac{1}{k^2}k^\nu(q^\alpha k^\mu-k\cdot qg^{\alpha\mu}),\end{aligned}\tag{C6}$$

which retains all the terms of $\tilde{\Gamma}^{\alpha,\mu\nu}$. In fact, since the q^μ and k^ν terms do not contribute after being multiplied with the boson polarization vectors, $\tilde{\Gamma}^{\alpha,\mu\nu}_2$ gives results identical to that of $\tilde{\Gamma}^{\alpha,\mu\nu}$ in the calculation.

When we consider the Pomeron exchange model of Sec. III, we obtain the gauge invariant amplitude (3.8) by applying the projection operator $\mathcal{P}_{\mu\nu}$ to the $\bar{\Gamma}^{\alpha,\mu\nu}$ of Eq. (3.5). One may, however, use the projection operators $\mathcal{P}^{\mu\nu}_{(l)}$ and $\mathcal{P}^{\mu\nu}_{(r)}$ to get

$$\begin{aligned}\bar{\Gamma}^{\alpha,\mu\nu}\to\Gamma^{\alpha,\mu\nu}_2&=\mathcal{P}^{\mu\mu'}_{(l)}\bar{\Gamma}^\alpha_{\mu'\nu'}\mathcal{P}^{\nu'\nu}_{(r)}\\&=(k+q)^\alpha g^{\mu\nu}-2k^\mu g^{\alpha\nu}-2q^\nu g^{\alpha\mu}\\&\quad-\frac{k\cdot q}{k^2q^2}(k+q)^\alpha q^\mu k^\nu\\&\quad-\frac{q^\mu}{q^2}\{k^\alpha q^\nu-q^\alpha q^\nu-2k\cdot qg^{\alpha\nu}\}\\&\quad-\frac{k^\nu}{k^2}\{q^\alpha k^\mu-k^\alpha k^\mu-2k\cdot qg^{\alpha\mu}\},\end{aligned}\tag{C7}$$

where the last three terms vanish after being multiplied with the boson polarization vectors although they are required to ensure gauge invariance. Note the close similarity between the amplitudes $\Gamma^{\alpha,\mu\nu}$'s.

A different choice of the gauge invariant $\Gamma^{\alpha,\mu\nu}$'s as given in Eqs. (3.8), (C3), (C6), and (C7) will necessitate the use of a different form for T_0 [56]. However, these different forms of T_0's will be related to each other as they are required to describe the unpolarized cross section. As it turns out, because of the incompleteness of our model, the $\Gamma^{\alpha,\mu\nu}$'s of Eqs. (C6) and (C7) have a singularity problem in the case of electroproduction as $k^2\to0$. In order to have a model for VDM amplitude which can be applied to electroproduction,

we use the $\Gamma^{\alpha,\mu\nu}$ of Eq. (3.8) with the T_0 of Eq. (3.11) in our calculation. To see the model dependence of our results, we carry out the calculations for the $\tilde{\Gamma}^{\alpha,\mu\nu}$ of Eq. (C2) as well.[10] Our results for $C_{zz}^{\rm BT}$ in these two models are shown in Fig. 17. One can see the close similarity of the two model predictions at small θ. This is true for the other spin observables as well, namely, they give nearly the same results in the kinematical region of our interest, say $\theta \leqslant 30°$. This is because the dominant contribution in this region comes from the $(k+q)^{\alpha} g^{\mu\nu}$ term, which is present in both models for VDM amplitude. As a conclusion, the model of this work gives the same predictions with those of Ref. [33] in the kinematical range of interest in this study.

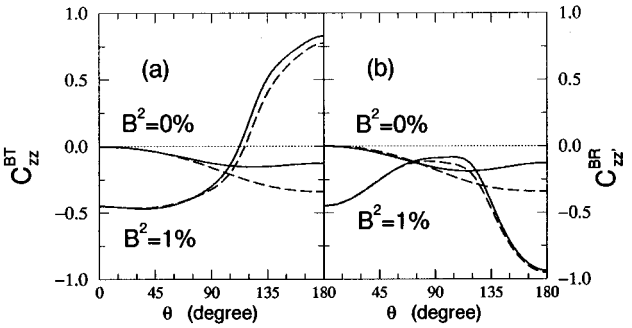

FIG. 17. Double polarization asymmetries (a) $C_{zz}^{\rm BT}$ and (b) $C_{zz'}^{\rm BR}$ for two models of $\Gamma^{\alpha,\mu\nu}$ with $B^2=0$ and 1%. The solid lines are obtained with $\Gamma^{\alpha,\mu\nu}$ of Eq. (3.8) and the dashed lines with $\tilde{\Gamma}^{\alpha,\mu\nu}$ of Eq. (C2). For simplicity, we take the phases $(\eta_0,\eta_1)=(+,+)$.

APPENDIX D: HELICITY AMPLITUDE IN VDM

In this Appendix, we give the details of the derivation for the helicity amplitude (3.15) of the VDM. We first define

$$\gamma_p = \frac{E_p^L}{M_N} \quad \text{and} \quad \gamma_p' = \frac{E_{p'}^L}{M_N}, \tag{D1}$$

which leads to

$$\alpha \equiv \frac{|\mathbf{p}|}{E_p^L + M_N} = \sqrt{\frac{\gamma_p - 1}{\gamma_p + 1}},$$

$$\alpha' \equiv \frac{|\mathbf{p}'|}{E_{p'}^L + M_N} = \sqrt{\frac{\gamma_p' - 1}{\gamma_p' + 1}}. \tag{D2}$$

Let $\mathbf{n}=\mathbf{p}/|\mathbf{p}|$ and $\mathbf{n}'=\mathbf{p}'/|\mathbf{p}'|$, we can then write

$$u_m(p) = \sqrt{\frac{\gamma_p+1}{2}} \begin{pmatrix} 1 \\ \alpha \boldsymbol{\sigma}\cdot\mathbf{n} \end{pmatrix} \chi_m, \tag{D3}$$

for the Dirac spinor of the proton with spin projection m, and a similar expression for $u_{m'}(p')$ for the outgoing proton.

Let us define $\mathcal{U}^{\alpha}$ as

$$\mathcal{U}^{\alpha} = \varepsilon_{\phi\mu}^{*} \Gamma^{\alpha,\mu\nu} \varepsilon_{\gamma\nu}. \tag{D4}$$

It is then straightforward to obtain

$$\overline{u}_{m_f}(p')\gamma_\mu u_{m_i}(p)\mathcal{U}^{\mu} = C\{[(1+\alpha\alpha'\mathbf{n}'\cdot\mathbf{n})\mathcal{U}^0 - \mathbf{a}\cdot\boldsymbol{\mathcal{U}}]\delta_{m_f m_i} + i[\alpha\alpha'(\mathbf{n}'\times\mathbf{n})\mathcal{U}^0 - (\mathbf{b}\times\boldsymbol{\mathcal{U}})]\cdot\langle m_f|\boldsymbol{\sigma}|m_i\rangle\}, \tag{D5}$$

where we have used $\mathbf{a}\equiv\alpha'\mathbf{n}'+\alpha\mathbf{n}$, $\mathbf{b}\equiv\alpha'\mathbf{n}'-\alpha\mathbf{n}$, and $C=\sqrt{(\gamma_p+1)(\gamma_p'+1)}/2$.

With $\Gamma^{\alpha,\mu\nu}$ of Eq. (3.8), $\mathcal{U}^{\alpha}$ can be decomposed into

$$\mathcal{U}^{\alpha} = 2(\mathcal{V}^{\alpha} - \mathcal{W}^{\alpha}), \tag{D6}$$

with

$$\mathcal{V}^{\alpha} = k^{\alpha}(\varepsilon_{\phi}^{*}\cdot\varepsilon_{\gamma}), \quad \mathcal{W}^{\alpha} = (\varepsilon_{\phi}^{*}\cdot k)\varepsilon_{\gamma}^{\alpha}, \tag{D7}$$

where the identity $\overline{u}(p')\gamma_\mu u(p)(p-p')^{\mu}=0$ has been used in order to simplify the form of $\mathcal{V}^{\alpha}$. Then the Wigner-Eckart theorem enables us to write the VDM amplitude as the sum of the spin-conserving part and the spin-flip part as in Eq. (3.15).

Using explicit forms of boson polarization vectors in the c.m. frame, we further have

$$\mathcal{V}^{\mu} = -k^{\mu} d^{(1)}_{\lambda_\gamma,\lambda_\phi}(\theta)[1+(\gamma_\phi-1)\delta_{\lambda_\phi 0}], \tag{D8}$$

and

$$\mathcal{W}^{\mu} = \begin{cases} \left(0, \frac{1}{2}|\mathbf{k}|\sin\theta, \pm\frac{i}{2}|\mathbf{k}|\sin\theta, 0\right) & \lambda_\phi = \pm 1, \lambda_\gamma = \pm 1, \\ \left(0, -\frac{1}{2}|\mathbf{k}|\sin\theta, \pm\frac{i}{2}|\mathbf{k}|\sin\theta, 0\right) & \lambda_\phi = \pm 1, \lambda_\gamma = \mp 1, \\ \left(0, \frac{\mp 1}{\sqrt{2}M_\phi}|\mathbf{k}|(|\mathbf{q}| - q_0\cos\theta), \frac{-i}{\sqrt{2}M_\phi}|\mathbf{k}|(|\mathbf{q}| - q_0\cos\theta), 0\right) & \lambda_\phi = 0, \lambda_\gamma = \pm 1, \end{cases} \tag{D9}$$

where $\gamma_\phi \equiv E_\phi^L/M_\phi$, which is close to 1 in the kinematical range considered in this paper.

[10] This is the model adopted in Ref. [33].

APPENDIX E: KNOCKOUT AMPLITUDE FOR CONFIGURATION (III)

In this case the knockout amplitude is proportional to the matrix element

$$T_{fi}^{uud\,(\mathrm{III})} \propto iA^* b_1^{(\mathrm{III})} \sum_{i=1,2,3} \langle q[s\bar{s}]^1_{m_\phi} | \langle p'[uud]^{1/2}_{m_f} | j_\mu^{(i)} \varepsilon_\gamma^\mu | [\psi_{J_c} \otimes [s\bar{s}]^1]^{1/2}_{m_i} \rangle. \tag{E1}$$

For simplicity we consider only the uud-quark configuration with the orbital excitation ($\ell=1$) of the $[^2\mathbf{8,70}]$ multiplet with $s_{uud}=\frac{1}{2}$. Thus, we do not consider the configuration of $[^4\mathbf{8,70}]$ with $s_{uud}=\frac{3}{2}$ because the corresponding electromagnetic transitions are suppressed by the Moorhouse selection rule. The relevant uud-cluster wave function reads

$$\psi_{jm_c} = \langle \tfrac{1}{2} m 1 \nu | j_c m_c \rangle \tfrac{1}{2} [\psi^{MS}_{\ell,\nu}(\phi^{MS}\chi^{MS} - \phi^{MA}\chi^{MA}) + \psi^{MA}_{\ell,\nu}(\phi^{MS}\chi^{MA} + \phi^{MA}\chi^{MS})], \tag{E2}$$

where $\psi^g_{\ell,\nu}$ is the radial wave function, and ϕ^g and χ^g are the flavor and spin wave functions, respectively. The superscript g ($=MS, MA$) specifies the symmetric property of the state with respect to the permutation $1\leftrightarrow 2$. Using the Jacobian coordinates of Ref. [66], i.e., $\xi_2 \sim x_1 - x_2$ and $\xi_2 \sim (x_1 + x_2)/2 - x_3$, each part of Eq. (E2) reads:

$$\psi_1^{MS} = \psi_1(\xi_1)\,\psi_0(\xi_2), \quad \psi_1^{MA} = \psi_0(\xi_1)\,\psi_1(\xi_2),$$

$$\phi^{MS} = \frac{1}{\sqrt{6}}(udu + duu - 2uud), \quad \phi^{MA} = \frac{1}{\sqrt{2}}(udu - duu),$$

$$\chi^{MS}_{1/2} = \frac{1}{\sqrt{6}}(\uparrow\downarrow\uparrow + \downarrow\uparrow\uparrow - 2\uparrow\uparrow\downarrow),$$

$$\chi^{MA}_{1/2} = \frac{1}{\sqrt{2}}(\uparrow\downarrow\uparrow - \downarrow\uparrow\uparrow). \tag{E3}$$

The three-quark proton wave function in this convention has the form

$$\psi_{1/2,m_p} = \frac{1}{\sqrt{2}}[\psi^S_{\ell=0}(\phi^{MS}\chi^{MS} + \phi^{MA}\chi^{MA})]. \tag{E4}$$

Then it is straightforward to show that the magnetic transition matrix element between the two uud states is

$$\begin{aligned}\mathrm{M.E.} &= \langle \psi_{1/2,m_f} | \sum_{j=1,2,3} \frac{e_j \boldsymbol{\sigma}_j}{2M_u} e^{-ik\cdot x_j} | \psi_{j_c,m_c} \rangle \cdot (\mathbf{k}\times\boldsymbol{\varepsilon}_\gamma) \\ &= \frac{1}{2M_u} \langle \psi_{1/2,m_f} | e_3 \boldsymbol{\sigma}_3 e^{-ik\cdot x_3} | \psi_{j_c,m_c} \rangle \cdot (\mathbf{k}\times\boldsymbol{\varepsilon}_\gamma),\end{aligned} \tag{E5}$$

which leads to

$$\begin{aligned}\mathrm{M.E.} = -i\frac{3E^L_\gamma}{2M_u}\frac{\lambda_\gamma\sqrt{3}}{2\sqrt{2}} \sum \langle \tfrac{1}{2} m 1 \nu | j_c m_c \rangle \langle \tfrac{1}{2} m 1 \lambda_i | \tfrac{1}{2} m_f \rangle \langle \psi^S_{\ell=0} | e^{-ik\cdot x_3} | \psi^{MS}_{\ell=1,\nu} \rangle \\ \times \langle \phi^{MS}\chi^{MS} + \phi^{MA}\chi^{MA} | e_3\sigma_3^z | \phi^{MS}\chi^{MS} - \phi^{MA}\chi^{MA} \rangle.\end{aligned} \tag{E6}$$

Then the spin-flavor part of the matrix element can be evaluated to be $2e/3$. The spatial matrix element can be calculated using the standard techniques of the RHOQM, e.g., as in Ref. [30].

[1] J. F. Donoghue and C. R. Nappi, Phys. Lett. **168B**, 105 (1986).
[2] J. Gasser, H. Leutwyler, and M. E. Sainio, Phys. Lett. B **253**, 252 (1991).
[3] EM Collaboration, J. Ashman *et al.*, Nucl. Phys. **B328**, 1 (1989).
[4] SM Collaboration, D. Adams *et al.*, Phys. Lett. B **329**, 399 (1994).
[5] E143 Collaboration, K. Abe *et al.*, Phys. Rev. Lett. **74**, 346 (1995).
[6] L. A. Ahrens *et al.*, Phys. Rev. D **35**, 785 (1987).
[7] E. J. Beise and R. D. McKeown, Comments Nucl. Part. Phys. **20**, 105 (1991).
[8] J. Ellis, E. Gabathuler, and M. Karliner, Phys. Lett. B **217**, 173 (1989).
[9] M. Anselmino and M. D. Scadron, Phys. Lett. B **229**, 117 (1989).
[10] H. J. Lipkin, Phys. Lett. B **256**, 284 (1991).
[11] D. B. Kaplan and A. Manohar, Nucl. Phys. **B310**, 527 (1988).
[12] R. D. McKeown, Phys. Lett. B **219**, 140 (1989).

[13] E. M. Henley, G. Krein, S. J. Pollock, and A. G. Williams, Phys. Lett. B **269**, 31 (1991).
[14] D. B. Kaplan, Phys. Lett. B **275**, 137 (1992).
[15] M. J. Musolf, T. W. Donnelly, J. Dubach, S. J. Pollock, S. Kowalski, and E. J. Beise, Phys. Rep. **239**, 1 (1994).
[16] T. Morii, A. I. Titov, and T. Yamanishi, Phys. Lett. B **375**, 343 (1996); **389**, 767(E) (1996).
[17] ASTERIX Collaboration, J. Reifenröther *et al.*, Phys. Lett. B **267**, 299 (1991).
[18] Crystal Barrel Collaboration, C. Amsler *et al.*, Phys. Lett. B **346**, 363 (1995).
[19] OBELIX Collaboration, A. Bertin *et al.*, Phys. Lett. B **388**, 450 (1996).
[20] S. B. Gerasimov, Phys. Lett. B **357**, 666 (1995); Chin. J. Phys. **34**, 848 (1996).
[21] C. B. Dover and P. M. Fishbane, Phys. Rev. Lett. **62**, 2917 (1989).
[22] J. Ellis, M. Karliner, D. E. Kharzeev, and M. G. Sapozhnikov, Phys. Lett. B **353**, 319 (1995).
[23] J. Ellis and M. Karliner, CERN Report No. CERN-TH/95-334, invited lectures at the International School of Nucleon Spin Structure, Erice, 1995, hep-ph/9601280.
[24] T. Gutsche, A. Faessler, G. D. Yen, and S. N. Yang, Nucl. Phys. B (Proc. Suppl.) **56A**, 311 (1997).
[25] Y. Lu, B. S. Zou, and M. P. Locher, Z. Phys. A **345**, 207 (1993); H. J. Lipkin and B.-S. Zou, Phys. Rev. D **53**, 6693 (1996); V. E. Markushin, Nucl. Phys. B (Proc. Suppl.) **56A**, 303 (1997).
[26] D. Buzatu and F. M. Lev, Phys. Lett. B **329**, 143 (1994).
[27] E. M. Henley, G. Krein, and A. G. Williams, Phys. Lett. B **281**, 178 (1992).
[28] E. M. Henley, T. Frederico, S. J. Pollock, S. Ying, G. Krein, and A. G. Williams, Few-Body Syst., Suppl. **6**, 66 (1992).
[29] A. I. Titov, Y. Oh, and S. N. Yang, Chin. J. Phys. **32**, 1351 (1994).
[30] A. I. Titov, S. N. Yang, and Y. Oh, Nucl. Phys. **A618**, 259 (1997).
[31] J. M. Laget, J. Korean Phys. Soc. **26**, S244 (1993).
[32] A. I. Titov, S. N. Yang, and Y. Oh, JINR-Communication E2-95-226, 1995.
[33] A. I. Titov, Y. Oh, and S. N. Yang, Phys. Rev. Lett. **79**, 1634 (1997).
[34] R. A. Williams, Phys. Rev. C **57**, 223 (1998).
[35] M. Alberg, J. Ellis, and D. Kharzeev, Phys. Lett. B **356**, 113 (1995); M. Alberg, Prog. Part. Nucl. Phys. **36**, 217 (1996).
[36] N. K. Pak and M. P. Rekalo, Eur. Phys. J. A **1**, 201 (1998).
[37] P. Joos *et al.*, Nucl. Phys. **B122**, 365 (1977).
[38] G. G. Ohlsen, Rep. Prog. Phys. **35**, 717 (1972).
[39] C. Bourrely, E. Leader, and J. Soffer, Phys. Rep. **59**, 95 (1980).
[40] H. E. Conzett, Rep. Prog. Phys. **57**, 1 (1994).
[41] F. Tabakin, Nucl. Phys. **A570**, 311c (1994); M. Pichowsky, Ç. Şavkli, and F. Tabakin, Phys. Rev. C **53**, 593 (1996).
[42] Ç. Şavkli, F. Tabakin, and S. N. Yang, Phys. Rev. C **53**, 1132 (1996).
[43] M. Jacob and G. C. Wick, Ann. Phys. (N.Y.) **7**, 404 (1959).
[44] C. G. Fasano, F. Tabakin, and B. Saghai, Phys. Rev. C **46**, 2430 (1992).
[45] D. G. Cassel *et al.*, Phys. Rev. D **24**, 2787 (1981).
[46] D. W. G. S. Leith, in *Electromagnetic Interactions of Hadrons*, Vol. 1, edited by A. Donnachie and G. Shaw (Plenum, New York, 1978), p. 345.
[47] A. Donnachie and P. V. Landshoff, Nucl. Phys. **B244**, 322 (1984); **B267**, 690 (1986).
[48] M. A. Pichowsky and T.-S. H. Lee, Phys. Lett. B **379**, 1 (1996); Phys. Rev. D **56**, 1644 (1997).
[49] A. Donnachie and P. V. Landshoff, Phys. Lett. B **185**, 403 (1987).
[50] P. V. Landshoff and O. Nachtmann, Z. Phys. C **35**, 405 (1987).
[51] A. Donnachie and P. V. Landshoff, Nucl. Phys. **B311**, 509 (1988/1989); Phys. Lett. B **296**, 227 (1992).
[52] J. R. Cudell, Nucl. Phys. **B336**, 1 (1990).
[53] S. V. Goloskokov, Phys. Lett. B **315**, 459 (1993).
[54] J.-M. Laget and R. Mendez-Galain, Nucl. Phys. **A581**, 397 (1995)
[55] J. R. Cudell and I. Royen, Phys. Lett. B **397**, 317 (1997); A. Hebecker and P. V. Landshoff, *ibid.* **419**, 393 (1998); M. Diehl, DAPNIA/SPhN, CEA/Saclay Report No. DAPNIA/SPhN-98-16, hep-ph/9803296.
[56] H. Fraas and D. Schildknecht, Nucl. Phys. **B14**, 543 (1969).
[57] J. D. Bjorken and S. D. Drell, *Relativistic Quantum Mechanics* (McGraw-Hill, New York, 1964).
[58] T. D. Lee and C. N. Yang, Phys. Rev. **128**, 885 (1962).
[59] H. J. Besch, G. Hartmann, R. Kose, F. Krautschneider, W. Paul, and U. Trinks, Nucl. Phys. **B70**, 257 (1974).
[60] J. Benecke and H. P. Dürr, Nuovo Cimento A **56**, 269 (1968).
[61] G. Wolf, Phys. Rev. **182**, 1538 (1969).
[62] A. I. Titov and Y. Oh, Phys. Lett. B **422**, 33 (1998).
[63] J. B. Bronzan, G. L. Kane, and U. P. Sukhatme, Phys. Lett. **49B**, 272 (1974).
[64] G. McClellan, N. Mistry, B. Sandler, J. Swartz, R. Talman, P. Walstrom, and G. Diambrini-Palazzi, Phys. Rev. Lett. **26**, 1597 (1971); H.-J. Halpern, R. Prepost, D. H. Tompkins, R. L. Anderson, B. Gottschalk, D. Gustavson, D. Ritson, G. Weitsch, and B. Wiik, *ibid.* **29**, 1425 (1972); J. Ballam *et al.*, Phys. Rev. D **7**, 3150 (1973); Omega Photon Collaboration, M. Atkinson *et al.*, Z. Phys. C **27**, 233 (1985).
[65] M. M. Lowry, BNL Report No. BNL-64156, 1997 (unpublished); T. Nakano *et al.*, Bull. Korean Phys. Soc. **15**, No. 2&3, 23 (1997); H. Gao (spokesperson), Jlab proposal.
[66] F. E. Close, *An Introduction to Quarks and Partons* (Academic, London, 1979).